IOP Publishing Rep. Prog. Phys. 89 (2026) 018002 https://doi.org/10.1088/1361-6633/ae2888

Reports on Progress in Physics

PAPER

RECEIVED
15 September 2025

REVISED
17 November 2025

ACCEPTED FOR PUBLICATION
5 December 2025

PUBLISHED
2 January 2026

Schwinger–Keldysh nonperturbative field theory of open quantum systems beyond the Markovian regime: application to spin-boson and spin-chain-boson models

Felipe Reyes-Osorio[1,*], Federico García-Gaitán[1], David J Strachan[2], Petr Plecháč[3], Stephen R Clark[2] and Branislav K Nikolić[1,*]

[1] Department of Physics and Astronomy, University of Delaware, Newark, DE 19716, United States of America
[2] H. H. Wills Physics Laboratory, University of Bristol, Bristol BS8 1TL, United Kingdom
[3] Department of Mathematical Sciences, University of Delaware, Newark, DE 19716, United States of America
[*] Authors to whom any correspondence should be addressed.

E-mail: freyes@udel.edu and bnikolic@udel.edu

Keywords: open quantum systems, non-Markovian, Schwinger–Keldysh, spin-boson, spin chain, nonperturbative

Corresponding editor: Dr Lorna Brigham

Abstract

We develop a unified framework for open quantum systems composed of many mutually interacting quantum spins, or any isomorphic systems like qubits and qudits, surrounded by one or more independent bosonic baths. Our framework, based on Schwinger–Keldysh field theory (SKFT), can handle arbitrary spin value S, dimensionality of space, and geometry, while being applicable to a large parameter space for system and bath. It can probe regimes in which *non-Markovian dynamics* and nonperturbative effects pose formidable challenges for other state-of-the-art theoretical methods. This is achieved by working with the two-particle irreducible (2PI) effective action, which resums classes of Feynman diagrams of SKFT to an infinite order. Furthermore, such diagrams are generated via an expansion in $1/N$, where N is the number of Schwinger bosons we employ to map spin operators onto canonically commuting ones, rather than via conventional expansion in system-bath coupling constant. We carefully benchmark our SKFT+2PI-computed results vs. numerically (quasi)exact ones from tensor network calculations applied to the archetypical spin-boson model where both methodologies are applicable. Additionally, we demonstrate the capability of SKFT+2PI to handle a much more complex spin-chain-boson model with multiple baths interacting with each spin where no benchmark from other methods is available at present. The favorable numerical cost of solving integro-differential equations produced by the SKFT+2PI framework with an increasing number of spins and time steps makes it a promising route for simulating driven-dissipative systems in quantum computing, quantum magnonics, and quantum spintronics.

1. Introduction

The conventional approach to open quantum system dynamics [1–5] formulates quantum master equations (QMEs) that evolve the reduced density operator of the subsystem of interest via equations that are, in general, integro-differential. The Markovian regime is typically well-described by time-local (i.e. differential) equations, often in the Lindblad form [6, 7]. On the other hand, the more demanding non-Markovian regime [3, 4, 8] usually requires time-nonlocal (i.e. integro-differential) equations [9, 10], or handling additional intricacies to preserve time-locality [2, 11–14]. For many-body systems, the operators within QMEs are usually expressed as polynomials of creation/annihilation operators acting in an exponentially increasing Hilbert space, so that a full matrix representation of the QME quickly becomes intractable by brute force methods. For example, even for a small number N_S of quantum spins of $S = 1/2$ or, equivalently, qubits, the size of matrices $2^{N_S} \times 2^{N_S}$ within QME is prohibitively computationally expensive.

The Markovian limit is characterized by time evolution that depends only on its present state and not on its history. It *requires* that system-environment coupling is weak and that environment correlations are short compared to the timescale of the system evolution (see [7] and section 5.1 for quantitative criteria involving these parameters to differentiate [3, 4, 8] Markovian vs. non-Markovian regimes). For Markovian QMEs where the system contains noninteracting degrees of freedom, so its Hamiltonian is quadratic in creation/annihilation operators, and the dissipative Lindbladian [6, 7] operators are linear in creation/annihilation operators, specialized techniques like 'third quantization' [15–17] can dramatically reduce the computational cost—for example, for noninteracting fermions, third quantization replaces $4^{N_e} \times 4^{N_e}$ matrices required in brute force methods with much more manageable $4N_e \times 4N_e$ matrices. Beyond such special cases, the search for polynomially scaling algorithms that can solve many-body Lindblad QME beyond quadratic Hamiltonians has recently led to the development [18, 19] of methods based on nonequilibrium quantum field theory in both functional integral [20–24] and second-quantization formulation [25]. In particular, the functional integral [20, 23] formulation of Schwinger–Keldysh field theory (SKFT) offers a convenient starting point for calculating expectation values (EVs) and correlation functions of various observables [19, 24], as well as a plethora of field-theoretic tools [18, 20, 23] developed within elementary particle physics. Indeed, SKFT was originally developed for problems in high-energy physics and cosmology [21–23] and later applied to low-energy physics [20, 24]. Such SKFT for open quantum systems has been applied to a number of dissipative and/or driven problems [26] in condensed matter and atomic-molecular-optical physics. However, while SKFT can, in principle, deal with both Markovian and non-Markovian systems on equal footing, prior works have mostly focused *only* on the Markovian regime [17–19, 24, 26, 27] by building Lindbladian evolution into the functional integral.

On the other hand, many open quantum systems, including notably quantum computers where a dissipative and noisy environment limits operational time of qubits [35, 36], exhibit pronounced memory effects and thereby time-retarded dynamics. A hallmark of such a non-Markovian regime is the revival of genuine quantum properties, such as quantum coherence, correlations, and entanglement [3, 4]. Such effects are enabled by backflow of information from the environment to the system. The ability to efficiently simulate non-Markovian open quantum systems also opens new avenues for their optimal control [37], including via environmental engineering [38]. However, non-Markovian open quantum systems exhibit exponential growth of complexity with the memory time of the environment, in quite analogous way to how complexity of closed quantum many-body systems grows with the number of degrees of freedom. This generally restricts many methods developed for the non-Markovian dynamics to *minimal* system sizes; or, if they can handle larger systems [39–44], they are typically restricted in evolution times, choice of environment(s) [40, 41, 44] and spatial geometry [39, 42–44].

Thus, these unresolved challenges call for exploration of alternative avenues that could allow one to handle many mutually interacting quantum degrees of freedom, each of which is strongly coupled to possibly *multiple* [34] structured environments. In addition, to describe experimentally relevant systems in quantum computing [35, 36, 45] or quantum spintronics [46–50] and quantum magnonics [51], one needs to evolve for sufficiently long and experimentally relevant times while handling arbitrary spatial dimensionality (including three-dimensional systems [45, 51]) and geometry [52] of both the degrees of freedom and their environments.

In this study, we introduce a field-theoretic approach offering such capabilities. Our approach combines SKFT with a two-particle irreducible (2PI) effective action [22, 53–57] that sums [58, 59] classes of Feynman diagrams to infinite order. The Feynman diagrams in our SKFT+2PI approach are obtained *not* from conventional perturbative expansion in the system-bath coupling constant, but instead from expansion in powers of a nonphysical small parameter $1/N$, where N is the number of Schwinger bosons we employ to map spin operators onto canonically commuting ones. This approach makes it possible to reach regimes that are *non-perturbative* in the system-environment coupling constant. Although both $1/N$ expansion and 2PI resummation techniques were originally developed long ago for problems in high-energy physics [23, 60, 61], with the understanding that $1/N$ expansion itself provides a non-perturbative resummation of the conventional perturbation theory, it is only recently [62] that a more profound understanding of how the $1/N$ expansion captures non-perturbative effects has been achieved. For example, in many problems, $1/N$ expansion generates [62] terms of a resurgent transseries [63, 64] in the system-bath coupling constant.

Our SKFT+2PI approach is developed for a general system of many quantum spins of length S, with arbitrary geometry and spatial dimensionality, which interact with each other and with one or many environments composed of infinitely many bosonic modes (figure 1 and equation (1)). Note that [55] and [56] have already employed a similar combination of SKFT, 2PI and $1/N$ expansions to study *closed* systems of quantum spins. Since such closed system dynamics is a limiting case of our more general

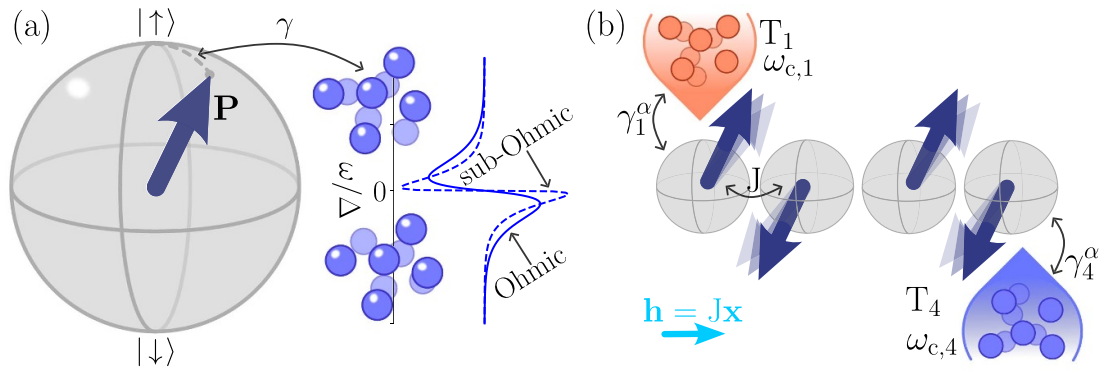

Figure 1. (a) Illustration of the spin-boson model (equation (2)) in which a two-level system, such as spin $S = 1/2$ or a qubit, interacts via a system-bath coupling constant γ with a dissipative environment modeled as a bosonic bath with infinite frequency content [28, 29]. The bath spectral density is given by equation (3), where $s = 1$ is Ohmic, $0 < s < 1$ is sub-Ohmic, and $s > 1$ is super-Ohmic. The high-frequency content of the bath decays exponentially and is characterized by a cutoff frequency ω_c. The state of the two-level system is uniquely determined by the Bloch vector $\mathbf{P}$, so that $|\mathbf{P}|$ quantifies the purity of the mixed quantum state [30, 31]. (b) Illustration of the spin-chain-boson model (equation (4)) in which a chain of $N_S = 4$ spins $S = 1/2$ interact with each other, and can couple to multiple independent baths per spin [32–34]. In the chosen system, each component of the spin at the edge of the chain couples to a separate bosonic bath kept at temperatures T_1 on the left edge and T_4 on the right edge, with $T_1 > T_4$ causing thermal transport carried by spin excitations.

SKFT+2PI for open quantum systems, in section 5.4 we provide comparison of SKFT+2PI vs. exact results for a small closed system of quantum spins, revealing failure of the former over relatively short time scales. In contrast, our SKFT+2PI for open quantum systems matches surprisingly well numerically (quasi)exact tensor network (TN) methods developed recently. In particular, we carefully benchmark our SKFT+2PI calculations against: the Lindblad QME describing the Markovian dynamics; or methods for non-Markovian dynamics including hierarchical equations of motion (HEOM) [65] and TN methods implemented as the time-evolving density operator with orthogonal polynomials algorithm (TEDOPA) [66–68] or the time-evolving matrix product operator (TEMPO) [40, 69]. Our results demonstrate that SKFT+2PI can replicate results of these four methods in a large region of the system and bath parameter space. Thus, our SKFT+2PI is a promising *unified framework* for open quantum systems even in the presence of strong interactions and non-Markovian effects. The related recent efforts include [57], where SKFT and 2PI are combined to study open systems of spins $S = 1/2$, but mostly in the Markovian regime.

To demonstrate the capability of our SKFT+2PI approach to probe nonperturbative and non-Markovian features of open quantum systems, we apply it to the *spin-boson* model (figure 1(a)) as an archetypical problem in the field of open quantum systems [1, 28, 70]. Despite its apparent simplicity (equation (2)), it contains plenty of challenges in the non-Markovian regime that have ignited the development of numerous specialized approaches [66–86]. Furthermore, by applying our SKFT+2PI to a much more complicated *spin-chain-boson* model (figure 1(b)), we demonstrate that it can tackle the previously unsolved problem of multiple independent environments coupled to noncommuting spin operators [39–44, 84]. For both problems, we study the dynamics of spin EVs, as well as multitime two-spin correlators. In contrast, the knowledge of the reduced density operator obtained from conventional QME approaches [1, 9, 10, 65, 87] is *insufficient* [39, 40] to obtain multitime correlators.

The paper is organized as follows. The general Hamiltonian on which our SKFT+2PI approach is demonstrated is presented in section 2; the spin-boson and spin-chain-boson models are discussed as particular cases of it in sections 2.1 and 2.2, respectively. Standard methods for solving the spin-boson model are overviewed in section 3, where we also provide details of specific algorithms among those that we employ as benchmarks. In sections 4 and 4.2, the SKFT+2PI theory and its numerical implementation are developed, while section 4.3 discusses how initial conditions are handled. Results obtained with SKFT+2PI for various regimes and specific models are shown in section 5. We conclude in section 6.

2. Models

To make the discussion transparent, we focus on a specific and general Hamiltonian

$$\hat{H} = \mathbf{h} \cdot \sum_n \hat{\mathbf{s}}_n + \sum_{nn'} J^{\alpha\beta}_{nn'} \hat{s}^\alpha_n \hat{s}^\beta_{n'} + \sum_{nk} \omega_{nk} \hat{\mathbf{b}}^\dagger_{nk} \hat{\mathbf{b}}_{nk} + \sum_{n\alpha k} g^\alpha_{nk} \hat{s}^\alpha_n \left(\hat{b}^{\alpha\dagger}_{nk} + \hat{b}^\alpha_{nk} \right), \tag{1}$$

where $\hat{\mathbf{s}}_n = (\hat{s}_n^x, \hat{s}_n^y, \hat{s}_n^z)^{\mathrm{T}}$ are operators for localized quantum spins of length S at sites $n = 1 \ldots N_S$ that are mutually interacting via the generalized Heisenberg exchange $J_{nn'}^{\alpha\beta}$ and are subject to an external magnetic field $\mathbf{h}$. The system of localized quantum spins $\hat{\mathbf{s}}_n$ is surrounded by an environment composed of many three-dimensional isotropic quantum harmonic oscillators of frequencies ω_{nk} whose canonical bosonic operators are $\hat{\mathbf{b}}_{nk} = (\hat{b}_{nk}^x, \hat{b}_{nk}^y, \hat{b}_{nk}^z)^{\mathrm{T}}$. Here, $\hat{\mathbf{b}}_{nk}$ and ω_{nk} correspond to the kth oscillator coupled to the nth spin via the in-general anisotropic coupling g_{nk}^{α}, Cartesian components are denoted by superscript $\alpha = x, y, z$ and $\hbar = 1$ for simplicity of notation.

2.1. Spin-boson model

A special case of the general Hamiltonian in equation (1) describing a single two-level quantum system—such as a spin $S = 1/2$, a qubit [35, 36], or any two well-separated energy levels [3, 4]—which is made open by its interaction with a bosonic bath composed of infinitely many harmonic oscillators is known as the spin-boson model [28]. This model is schematically illustrated in figure 1(a). The Hamiltonian of the spin-boson model is obtained for $N_S = 1$ spin of length $S = 1/2$ by setting the external magnetic field to $\mathbf{h} = (\Delta, 0, \omega_q)$, the Heisenberg exchange to $J_{11}^{\alpha\beta} = 0$, and all spin-bath couplings are set to zero except for $g_{1k}^z = g_k$. This leads to simplification of the general Hamiltonian in equation (1) into

$$\hat{H} = \omega_q \hat{s}^z + \Delta \hat{s}^x + \sum_k \omega_k \hat{b}_k^\dagger \hat{b}_k + \hat{s}^z \sum_k g_k \left(\hat{b}_k + \hat{b}_k^\dagger \right). \tag{2}$$

Here, $\hat{s}^\alpha$ are the Pauli operators; ω_q is the energy difference between the two eigenstates of $\hat{s}^z$, $\hat{s}^z|\uparrow\rangle = |\uparrow\rangle$, $\hat{s}^z|\downarrow\rangle = -|\downarrow\rangle$; Δ is the tunneling matrix element, which also sets the units of energy; and we suppress the subscript n since there is only one spin. The properties of the bath are fully captured by the coupling-weighted spectral density, $\mathcal{J}(\omega) = 2\pi \sum_k g_k^2 \delta(\omega - \omega_k)$, for which a generic form

$$\mathcal{J}(\omega) = \gamma \omega_{\mathrm{c}}^{1-s} \omega^s \mathrm{e}^{-\omega/\omega_{\mathrm{c}}}, \tag{3}$$

is usually assumed [28, 29]. Here γ is a single parameter characterizing the system-bath coupling strength; ω_{c} is the cutoff frequency of the bath signifying the exponential decay of the high-frequency content; parameter $0 < s < 1$, $s = 1$ and $s > 1$ classifies spectral densities as sub-Ohmic, Ohmic, and super-Ohmic, respectively [74]; and the spectral density $\mathcal{J}(-\omega) = -\mathcal{J}(\omega)$ is antisymmetrically extended [71].

Although the spin-boson model has been intensely studied for many decades [28], its non-Markovian dynamics [3, 8, 66, 88, 89] still pose a formidable challenge despite the plethora of available numerical and analytical methods [66–82, 84–86] for open quantum systems developed specifically for it. This is especially true for the case of zero [70, 74, 89] or ultralow temperatures and/or specific frequency content of the bosonic bath [74, 88]. For example, the sub-Ohmic case at zero temperature, with a relatively large portion of low-frequency modes (figure 1(a)), is considered particularly challenging [74, 78–81, 85] and of relevance to superconducting qubits [35, 36, 45] subjected to electromagnetic noise [80]. Other challenges are, in general, posed by the long-time limit [74, 85, 86, 90] of non-Markovian dynamics [88, 89], whose memory effects force information to flow from the environment back into the system. Such effects are not necessarily transient [88]. It is generically assumed that the non-Markovian regime [3, 4, 8] in open quantum system dynamics is entered when the system-bath coupling is sufficiently strong and correlations of the bath do not decay rapidly [7]. But detailed examination [88, 89] of measures of non-Markovianity vs. system-bath coupling strength in the case of the spin-boson model shows complex nonmonotonic dependence, including sensitivity to the cutoff frequency ω_{c}, temperature T and frequency content of the bath.

2.2. Spin-chain-boson model

Another special case of the general Hamiltonian in equation (1) is obtained by considering $N_S > 1$ spins with Heisenberg exchange coupling between the nearest neighbors $J_{n,n+1}^{\alpha\alpha} = J_{n,n-1}^{\alpha\alpha} = J/2$ and with each component $\alpha = x, y, z$ of the spins at the ends of the chain being coupled to independent bosonic baths (figure 1(b)). Such coupling to the environment is described by setting all spin-bath couplings to zero except for g_{1k}^{α} and $g_{N_S k}^{\alpha}$. An external magnetic field along the x-axis is included by using $\mathbf{h} = (h, 0, 0)$, and coupling between spins is ferromagnetic (FM) if $J < 0$ and antiferromagnetic (AF) if $J > 0$. Thus, the Hamiltonian of such spin-chain-boson model is given by $\hat{H} = \hat{H}_{\mathrm{S}} + \hat{H}_{\mathrm{B}}$, where

$$\hat{H}_{\mathrm{S}} = \sum_n \left(J \hat{\mathbf{s}}_n \cdot \hat{\mathbf{s}}_{n+1} + h \hat{s}_n^x \right), \tag{4a}$$

$$\hat{H}_{\mathrm{B}} = \sum_{n=1,N_S} \sum_{k} \left[\omega_{nk} \hat{\mathbf{b}}^{\dagger}_{nk} \hat{\mathbf{b}}_{nk} + \sum_{\alpha} g^{\alpha}_{nk} \hat{s}^{\alpha}_{n} \left(\hat{b}^{\alpha\dagger}_{nk} + \hat{b}^{\alpha}_{nk} \right) \right]. \tag{4b}$$

The frequency content of the bosonic baths is assumed to be described by the spectral density in equation (3), but with independent temperatures T_n, cutoff frequencies $\omega_{c,n}$, exponents s_n, and system-bath couplings γ^{α}_{n} for $n=1$ and $n=N_S$. The couplings γ^{α}_{n} are further assumed to be independent for each spin component α, thus allowing for anisotropically coupled baths.

This spin-chain-boson model represents a challenge to recently developed approaches [39–44, 84] for non-Markovian dynamics due to its larger Hilbert space and multiple [34] bosonic environments coupled to non-commuting operators. Interestingly, prior studies of open quantum magnets in equilibrium have found that ordinarily forbidden long-range order in one-dimensional (1D) quantum spin chains can be stabilized by the presence of Ohmic and sub-Ohmic baths [91]. Thus, having a formalism that can examine non-Markovian dynamics of standard or exotic quantum magnets (such as quantum spin liquids [92]), or systems of interacting qubits [35, 36] including their arrangements in three-dimensional geometries [45], is of great contemporary interest, as they are necessarily interacting with a dissipative environment at finite temperature in experiments [93]. While methods based on TNs can be applied to systems similar to the spin-chain-boson model when the coupling to the bath is simplified [39, 40], no standard approach for non-Markovian dynamics in systems with more complicated bath structures (such as the one assumed in this work or with faster entanglement growth occurring in higher spatial dimensions) has emerged thus far.

3. Standard methods for solving the spin-boson model

For solving the spin-boson model described in section 2.1, the brute force numerical solution of QME in the non-Markovian regime requires computing high-dimensional integrals over time [87] stemming from time-dependent perturbation theory. Although this can be done for low-order terms in the expansion [94], the inclusion of higher-order terms makes the accuracy of calculations extremely sensitive to numerical errors. As an alternative, the widely used HEOM approach [65] has been developed by converting the time-nonlocal integro-differential QME of the brute force method [87] into a set of finitely many time-local differential equations. However, its standard version [65] is limited to high temperatures [95], which has motivated recent efforts to extend the HEOM approach [85, 86, 90] to access zero temperature and much longer simulation times. Multilayer multiconfiguration time-dependent Hartree (ML-MCTDH) [73, 74], numerical renormalization group [78–81], inchworm quantum Monte Carlo [96–98], self-consistent dynamical maps [83] and TN approaches [40, 41, 84, 99], that can handle non-Markovian dynamics at zero temperature have also been developed. However, HEOM and ML-MCTDH algorithms are prohibitively expensive for many interacting quantum spins or, equivalently, qubits [35, 36].

Since the spin-boson model offers a playground for benchmarking our SKFT+2PI approach vs. standard approaches, we overview in sections 3.1 and 3.2 HEOM and specific TN-based algorithms, respectively, that we employ. We also overview in section 3.3 the Lindblad QME we use as a benchmark in the weak system-bath coupling regime.

3.1. HEOM approach to non-Markovian dynamics

The HEOM algorithm [65], initially developed for problems in quantum chemistry [100], is a widely used method for solving QMEs of open quantum systems with arbitrary system-bath coupling. However, in its original formulation [65, 100] it requires finite temperature, $T>0$ [85, 86, 90, 95]. The non-perturbative treatment of interaction with the bath is achieved by introducing a hierarchy of auxiliary density matrices that encode system-bath correlations and entanglement [65, 101]. This hierarchy relies on the expansion of the bath correlation function into an exponential form. The limitations of the HEOM method are well known [85, 86, 90, 95] and arise from the truncation of either the number of auxiliary matrices (a stronger system-bath coupling requires a higher hierarchy cutoff), or the truncation in the exponential decomposition of the bath correlation (typically, lower temperature requires more terms in the expansion). The exact exponential expansion of an arbitrary spectral density $\mathcal{J}(\omega)$ of the bath is not known. We fit the spectral density in equation (3) using a sum of up to four underdamped [65] spectral densities whose exponential expansion is well known [102]. In order to guarantee convergence, we ran simulations varying the hierarchy cutoff, up to a maximum of 11. In addition, we also adjust the number of exponential terms, using a maximum of 16 terms for the lowest temperature case $k_{\mathrm{B}}T=0.1\Delta$ (figure 7), where k_{B} is the Boltzmann constant. All such calculations were performed using the HEOM extension [103] of the `QuTiP` [104, 105] package.

3.2. TN approach to non-Markovian dynamics

The TN approaches to non-Markovian dynamics of open quantum systems are broadly divided into two complementary classes [84]. One class, which hosts TEDOPA used in our study as a benchmark (figures 5, 7, and 9), is based on applying a thermofield chain mapping [66, 67]. This approach purifies a finite temperature environment and transforms its representation into a chain geometry ideally suited to matrix product state (MPS) algorithms. Then, the pure quantum state of the full system and environment is unitarily evolved using well established MPS techniques like the time-dependent variational principle (TDVP) [106, 107]. The other class is, instead, based on applying a MPO to describe the Feynman-Vernon influence functional in the temporal domain [40, 68–70, 108, 109]. Separating such representation of the Feynman-Vernon influence functional into contributions from the unitary dynamics and from different additive baths, each of which is represented by a process tensor (PT) leads to increased performance [39–41, 76, 110, 111]. TEMPO, the second TN-based benchmark we employ (figures 5, 7, and 9), belongs to this class.

When implementing TEDOPA the chain mapping representation of an environment spectral function is truncated to a finite length which places an upper limit on the time for which the dynamics faithfully captures the environment's continuum [112, 113]. However, this is rarely a practical issue since the computational cost of increasing the chain length scales linearly. Nonetheless the *strongest limitation* of TEDOPA is the short time evolution that can reached. The reason for this can be (i) the unfavorable scaling of the method with the local Hilbert space dimension of the bosonic modes when oscillators are highly excited, and (ii) the transient 'entanglement barrier' [114–116] that some dynamics can exhibit where the MPS bond dimension grows prohibitively quickly with time. For example, even Markovian dynamics can lead to a spike [117] of the many-body entanglement of the system, despite the presence of a dissipative environment and naïve expectation [118] that interactions with the environment should curtail entanglement growth. Recently, new approaches have been developed to overcome these issues, including a Markovian closure of the chain that accurately models the effects of the infinitely long truncated part of the chain [119], adaptive one-site TDVP which makes more efficient use of the bond dimension [120], and interaction-picture chain mapping that results in lower oscillation occupation in the environment [121]. For TEMPO and PT-TEMPO, there is a combination of Trotter errors and truncation errors from the compression of the MPS bond dimension whose interplay is not currently fully understood and, alas, also limits the reachable simulation times [108, 109].

For the spin-boson model (equation (2)) at ultralow temperatures, we use (figures 5(a), (c) and 7(a), (c)) TEDOPA, based on an MPS description of a thermofield-chain-mapped system [66, 67]. An MPS is a representation of an arbitrary pure state as a product of local tensors given by [122]

$$|\psi\rangle = \sum_{s_1,\ldots,s_N} A_1^{s_1}\ldots A_{N-1}^{s_{N-1}} A_N^{s_N} |s_1\ldots s_N\rangle, \tag{5}$$

where $A_j^{s_i}$ is a $\chi_j \times \chi_{j+1}$ matrix (with $\chi_1 = \chi_N = 1$ fixed) for the jth local degree of freedom possessing a d_j dimensional Hilbert space. The bond dimension χ_j is a crucial parameter controlling the expressiveness of the MPS ansatz and is directly related to the maximum bipartite entanglement it can support.

In order to represent the equilibrium state of the bath in the form of a pure state MPS, we use thermofield purification in which the finite temperature of the bath is encoded in two different baths at zero temperature [123]. The density operator of a bosonic bath at inverse temperature $\beta = 1/k_B T$ is given by

$$\hat{\rho}_\beta = \bigotimes_k \left(\sum_{n=0}^{\infty} \frac{e^{-\beta n \omega_k}}{Z_k} |n\rangle_k \langle n|_k \right), \tag{6}$$

where $Z_k = (1 - e^{-\beta\omega_k})^{-1}$; n is the occupation of mode k; and k_B is the Boltzmann constant. By introducing an identical auxiliary system A, with canonical operators $\hat{a}_k^\dagger, \hat{a}_k$ and Hamiltonian $H_A = -\sum_k \omega_k \hat{a}_k^\dagger \hat{a}_k$, we define the thermofield double state as a purification of $\hat{\rho}_\beta$, given by

$$\begin{aligned} |\Omega_\beta\rangle &= \bigotimes_k \left(\sum_{n=0}^{\infty} \sqrt{\frac{e^{-\beta n \omega_k}}{Z_k}} |n\rangle_k \otimes |n\rangle_k^A \right) \\ &= \exp\left(\sum_k \theta_k \left(\hat{b}_k \hat{a}_k - \hat{b}_k^\dagger \hat{a}_k^\dagger \right) \right) |\text{vac}\rangle. \end{aligned} \tag{7}$$

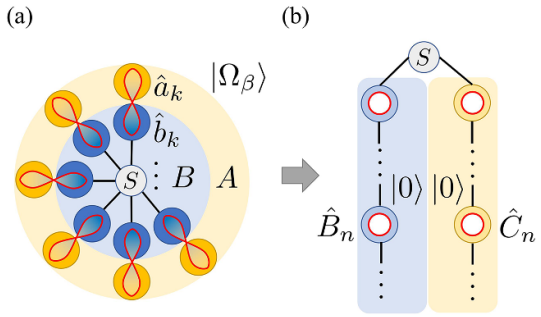

Figure 2. (a) Illustration of how thermofield purification of the initial thermal state of the bath entangles each bath eigenmode with an ancilla. The geometry of interactions of the spin S with the bath modes is a star. (b) After performing a Bogoliubov transformation and orthogonal polynomial tridiagonalization, we arrive at a two-chain geometry ideal for MPS calculations.

Here, $|\text{vac}\rangle$ is the bosonic vacuum state; $|n\rangle_k^A$ is a state of the k mode in the auxiliary system; $\theta_k = \text{atanh}(e^{-\beta\omega_k/2})$; and $\hat{\rho}_\beta = \text{Tr}_A|\Omega_\beta\rangle\langle\Omega_\beta|$ is recovered by partial trace over the states of auxiliary system A. The state $|\Omega_\beta\rangle$ is the vacuum for the modes

$$\hat{c}_{1,k} = \cosh(\theta_k)\,\hat{b}_k - \sinh(\theta_k)\,\hat{a}_k^\dagger, \tag{8}$$

$$\hat{c}_{2,k} = \cosh(\theta_k)\,\hat{a}_k - \sinh(\theta_k)\,\hat{b}_k^\dagger, \tag{9}$$

obtained from a thermal Bogoliubov transformation. In this new basis, the extended Hamiltonian is given by

$$\hat{H} = \omega_q\hat{s}^z + \Delta\hat{s}^x + \sum_k \omega_k\left(\hat{c}_{1,k}^\dagger\hat{c}_{1,k} - \hat{c}_{2,k}^\dagger\hat{c}_{2,k}\right) + \hat{s}^z\sum_k\left[g_{1k}\left(\hat{c}_{1,k} + \hat{c}_{1,k}^\dagger\right) + g_{2k}\left(\hat{c}_{2,k} + \hat{c}_{2,k}^\dagger\right)\right], \tag{10}$$

where $g_{1k} = g_k\cosh(\theta_k)$ and $g_{2k} = g_k\sinh(\theta_k)$.

As it stands, this setup has a star geometry in which the spin interacts with each mode of the bath, as illustrated graphically in figure 2(a). This corresponds to long-ranged interactions within a 1D representation of the system, which are more difficult to handle using MPSs. For this reason, we map via continuous mode tridiagonalization the two zero-temperature star geometry baths into two 1D tight-binding chains, each coupled to the system spin [66], as shown in figure 2(b). In the continuum representation, these two baths are characterized by spectral densities $\mathcal{J}_1(k) = [1 + n_{\text{BE}}(k)]\mathcal{J}(k)$ and $\mathcal{J}_2(k) = n_{\text{BE}}(k)\mathcal{J}(k)$, where $n_{\text{BE}}(k)$ is the Bose–Einstein distribution function. We then define new bosonic operators $\hat{B}_n$ and $\hat{C}_n$ such that

$$2\hat{c}_{1,k} = \sum_n U_{1,n}(k)\,\hat{B}_n, \qquad \hat{c}_{2,k} = \sum_n U_{2,n}(k)\,\hat{C}_n. \tag{11}$$

Here, $U_{j,n}(k) = g_j(k)\pi_{j,n}(k)/\rho_{n,j}$ for $j = 1,2$ and $\pi_{j,n}(k)$ are monic orthogonal polynomials that obey

$$\int_0^\infty \text{d}k\,\mathcal{J}_j(k)\,\pi_{j,n}(k)\,\pi_{j,m}(k) = \rho_{j,n}^2\delta_{n,m}, \tag{12}$$

with $\rho_{j,n}^2 = \int_0^\infty \text{d}k\,\mathcal{J}_j(k)\pi_{j,n}^2(k)$ [67]. This description simplifies significantly at zero temperature, as $\mathcal{J}_1(k) = 0$, so only one chain is needed. Using a finite cutoff of M modes for the mapping, we have

$$\begin{aligned}\hat{H} = {} & \omega_q\hat{s}^z + \Delta\hat{s}^x + \hat{s}^z\left[\rho_{1,0}\left(B_0 + B_0^\dagger\right) + \rho_{2,0}\left(C_0 + C_0^\dagger\right)\right] \\ & + \sum_{n=0}^{M}\left(\alpha_{1,n}\hat{B}_n^\dagger\hat{B}_n - \alpha_{2,n}\hat{C}_n^\dagger\hat{C}_n + \sqrt{\beta_{1,n+1}}\hat{B}_{n+1}^\dagger\hat{B}_n - \sqrt{\beta_{2,n+1}}\hat{C}_{n+1}^\dagger\hat{C}_n + \text{H.c.}\right),\end{aligned} \tag{13}$$

where the coefficients $\alpha_{j,n}$ and $\beta_{j,n}$ are defined through the recurrence relation $\pi_{j,n+1}(k) = (k - \alpha_{j,n})\pi_{j,n}(k) - \beta_{j,n}\pi_{j,n-1}(k)$, with $\pi_{j,-1}(k) = 0$. These chain parameters were generated using the `ORTHPOL` package [124]. Generically, they are found to quickly converge to constants $\alpha_{i,n} \to \alpha_i$, $\beta_{i,n} \to \beta_i$. Using the Lieb-Robinson bounds [112, 113], sites further than $\sim \tau\beta_i$ have a negligible effect on the system dynamics up to time τ, giving a well-defined measure of the length of bath chains we need. In this

sense, the discretization generated by orthogonal polynomials is exact up to a finite time. To time evolve the MPS, we use the two-site variant of the TDVP [106, 125–127] which dynamically updates the MPS bond dimensions to maintain a desired level of precision.

3.3. Lindblad QME approach to Markovian dynamics

In the weak system-bath coupling regime of the spin-boson model (equation (2)), where the system (i.e. spin) dynamics is expected to be Markovian [88, 89], the Lindblad QME [6, 7]

$$\frac{\mathrm{d}\hat{\rho}}{\mathrm{d}t} = -\mathrm{i}\left[\hat{H}_{\mathrm{S}}, \hat{\rho}\right] + \sum_{i=0}^{2}\left(\hat{L}_i\hat{\rho}\hat{L}_i^{\dagger} - \frac{1}{2}\left\{\hat{L}_i^{\dagger}\hat{L}_i, \hat{\rho}\right\}\right), \tag{14}$$

can accurately capture the open quantum system dynamics. Here $\hat{H}_{\mathrm{S}}$ is the Hamiltonian of an isolated spin, composed of the first two terms on the right-hand side (RHS) of equation (2); $\hat{\rho}$ is the spin density operator [30]; and $\hat{L}_i$ is a set of three Lindblad operators [6, 7] which account for the presence of the bosonic bath. Those three $\hat{L}_i$ operators for the spin-boson model can be expressed [1] in the energy eigenbasis of $\hat{H}_{\mathrm{S}}$, $\hat{H}_{\mathrm{S}}|\pm\rangle = E_{\pm}|\pm\rangle$, of $\hat{H}_{\mathrm{S}}$ as

$$\hat{L}_0 = \sqrt{J(\Delta E)\left[1 + n_{\mathrm{BE}}(\Delta E)\right]\left[\langle +|\hat{s}_z|-\rangle\right]^2}|-\rangle\langle +|, \tag{15a}$$

$$\hat{L}_1 = \sqrt{J(\Delta E)\, n_{\mathrm{BE}}(\Delta E)\left[\langle +|\hat{s}_z|-\rangle\right]^2}|+\rangle\langle -|, \tag{15b}$$

$$\hat{L}_2 = \sqrt{2\gamma_L T\langle -|\hat{s}_z|-\rangle\langle +|\hat{s}_z|+\rangle}|-\rangle\langle -|, \tag{15c}$$

where $\Delta E = E_+ - E_-$ is the energy difference of the two levels, and γ_L is the system-bath coupling. Note that γ_L has to be adjusted in figure 5 by hand to match SKFT+2PI- or TN-computed results.

4. SKFT + 2PI for open quantum spin systems

To define the functional integral of SKFT, it is convenient to first map the spin operators in the general Hamiltonian of equation (1) onto fermionic or bosonic operators [55, 56, 128] subject to canonical commutation relations, so that the Wick theorem and other field-theoretic machinery applicable to such operators can be utilized. Here we employ the Schwinger boson mapping [56, 129–131], in which operators of spin S are expressed using N flavors of bosons. Any spin length S can be represented by any number of Schwinger boson flavors N. Therefore, N is not a physical parameter; rather, it is an auxiliary object of the mathematical framework. For $N = 2$, which we use in this work to curtail computational complexity, the spin operators are expressed as

$$\hat{s}_n^{\alpha} = \frac{1}{2}\hat{\psi}_n^{\dagger}\boldsymbol{\sigma}^{\alpha}\hat{\psi}_n, \tag{16}$$

where $\boldsymbol{\sigma}^{\alpha}$ is a matrix representation of the Pauli operators, and $\hat{\psi}_n = (\hat{a}_n^{(1)}, \hat{a}_n^{(2)})^{\mathrm{T}}$ is a doublet of the two flavors of Schwinger bosons for spin n. Although other mappings from spin to bosons or fermions can be employed, Schwinger bosons preserve rotational symmetry, as opposed to Holstein–Primakoff bosons [132]; and are also generalizable to larger spin values S, unlike Majorana [55] or Jordan–Wigner [133] fermions applicable only to $S = 1/2$. The spin length S is set by constraining the Schwinger boson occupation at each site to be

$$\hat{a}_n^{(1)\dagger}\hat{a}_n^{(1)} + \hat{a}_n^{(2)\dagger}\hat{a}_n^{(2)} = 2S. \tag{17}$$

The constraint ensures that only a subspace of the infinite dimensional bosonic Hilbert space is utilized for spin dynamics. For example, the one-boson subspace corresponds to the physical Hilbert space of a spin $S = \frac{1}{2}$ spanned by $|1,0\rangle \equiv |\uparrow\rangle$ and $|0,1\rangle \equiv |\downarrow\rangle$. Similarly, the two-boson subspace corresponds to a spin $S = 1$, spanned by $|2,0\rangle \equiv |\uparrow\rangle$, $|1,1\rangle \equiv |0\rangle$, and $|0,2\rangle \equiv |\downarrow\rangle$; the three-particle subspace corresponds to $S = \frac{3}{2}$, and so forth [129, 130].

The Schwinger–Keldysh (SK) functional integral is formulated in terms of complex fields ψ_n which are complex eigenvalues

$$\hat{\psi}_n|\psi_1, \ldots \psi_n, \ldots \psi_{N_S}\rangle = \psi_n|\psi_1, \ldots \psi_n, \ldots \psi_{N_S}\rangle, \tag{18}$$

of $\hat{\psi}_n$, and whose corresponding eigenvectors $|\psi_1,\ldots\psi_n,\ldots\psi_{N_S}\rangle$ are the bosonic coherent states. Instead of working with complex-valued fields for the Schwinger bosons, we expand in terms of their real and imaginary parts, $a_n^{(\sigma)} = (x_n^{(\sigma)} + \mathrm{i}p_n^{(\sigma)})/\sqrt{2}$, which are grouped into the 4-component field

$$\varphi_n = \left(x_n^{(1)}, p_n^{(1)}, x_n^{(2)}, p_n^{(2)}\right)^{\mathrm{T}}. \tag{19}$$

Working with the real-valued fields φ_n simplifies the rules that generate the diagrammatic expansion of the 2PI action. Additionally, it manifests the $O(4)$ symmetry of the theory. Since an $O(2)$ theory, which has fewer fields, is already remarkably close to the large-N limit [134], we conclude that the usage of a $1/N$ expansion [61] is justified, despite only employing two flavors of complex Schwinger bosons.

The spin fields can be constructed as $s_n^\alpha = \varphi_n^{\mathrm{T}} K^\alpha \varphi_n/2$, where

$$K^x = \boldsymbol{\sigma}^x \otimes I_2, \quad K^y = -\boldsymbol{\sigma}^y \otimes \boldsymbol{\sigma}^y, \quad K^z = \boldsymbol{\sigma}^z \otimes I_2, \tag{20}$$

and I_2 is the 2×2 identity matrix. Then, the SK action, $S = S_S + S_B$, as one of the central quantities in SKFT, is given by

$$S_S = -\int_{\mathcal{C}} \mathrm{d}t \sum_n \varphi_n^{\mathrm{T}} \left(\frac{\mathrm{i}}{2} K^0 \partial_t + H\right) \varphi_n + \sum_{\alpha\beta nn'} J_{nn'}^{\alpha\beta} s_n^\alpha s_{n'}^\beta, \tag{21a}$$

$$S_B = \int_{\mathcal{C}} \mathrm{d}t \sum_{n\alpha k} \left[b_{nk}^{\alpha\star} \left(i\partial_t - \omega_{nk}\right) b_{nk}^\alpha - g_{nk}^\alpha s_n^\alpha \left(b_{nk}^\alpha + b_{nk}^{\alpha\star}\right)\right], \tag{21b}$$

where $\mathcal{C}$ is the SK closed time contour [21–24]. Here S_S and S_B are the contributions to the total action S from the system of spins and the bath, respectively; $K^0 = I_2 \otimes \boldsymbol{\sigma}^y$; and $H = \sum_\alpha h^\alpha K^\alpha/4$. For simplicity, we consider bosonic baths that are local, i.e. no more than a single spin can couple to a given bath. This does not preclude multiple baths from coupling to the same spin, which can also be straightforwardly generalized to nonlocal baths. Since S_B is in the Gaussian form, it can be integrated out exactly. The quartic term that is produced,

$$\propto s_n^\alpha(t)\, \Xi_n^\alpha(t,t')\, s_n^\alpha(t'), \tag{22}$$

is the so-called influence phase [29], and represents a *nonlocal-in-time* effective self-interaction of the spins generated by the presence of the bath. The bath kernel

$$\Xi_n^\alpha(t,t') = \sum_k \left(g_{nk}^\alpha\right)^2 B_{nk}^\alpha(t-t'), \tag{23}$$

is given in terms of the noninteracting GF of the bosonic bath

$$\mathrm{i}B_{nk}^\alpha(t,t') = \langle b_{nk}^\alpha(t)\, b_{nk}^{\alpha\star}(t')\rangle_0, \tag{24}$$

where $\langle\ldots\rangle_0$ is the EV [24] neglecting spin-bath and spin-spin coupling. The possibility of placing the two times t and t' on the forward and backward branches of the SK contour $\mathcal{C}$ makes $B_{nk}^\alpha(t,t')$ and any other GF of the theory contain four components [23, 24, 135, 136]. However, only two of those components are independent, motivating different expressions in terms of GFs that take real-time arguments. In condensed matter physics, it is common to use either the lesser $G^<$ and greater $G^>$ GFs, often employed in the second-quantized operator formulation of Keldysh GFs [135, 136]; or the retarded and Keldysh GFs, often employed in the equivalent functional integral formulation [24]. In this work, we will decompose contour GFs in terms of their Keldysh (K) and spectral (s) components [22], respectively expressed as

$$G^{K/s}(t,t') = G^>(t,t') \pm G^<(t,t'), \tag{25}$$

where $+$ sign is for G^K and $-$ sign is for G^s. The physical meaning of G^s is to describe the density of available states, while G^K describes how those states are occupied. The contour GFs are then reconstructed as

$$G(t,t') = \frac{1}{2} G^K(t,t') + \frac{1}{2} \mathrm{sgn}_{\mathcal{C}}(t,t')\, G^s(t,t'), \tag{26}$$

where the contour sign function $\mathrm{sgn}_{\mathcal{C}}(t,t')$ equals 1 if its arguments are ordered on the contour; -1 if its arguments are not ordered on the contour; and 0 if its arguments are the same. Through this decomposition, integrals over $\mathcal{C}$ simplify to become real-time causal integrals, which, otherwise, in the lesser/-greater representation [135, 137] require the usage of the much more demanding Langreth rules [138]. For the noninteracting GFs of the bosonic bath $B^{\alpha}_{nk}(t,t')$, closed expressions for $B^{\alpha,K/s}_{nk}$ are given by

$$B^{\alpha,K}_{nk}(t,t') = -\mathrm{i}\coth\left(\frac{\omega_{nk}}{2k_{\mathrm{B}}T_n}\right)\mathrm{e}^{-\mathrm{i}\omega_{nk}\left(t-t'\right)}, \tag{27a}$$

$$B^{\alpha,s}_{nk}(t,t') = -\mathrm{i}\mathrm{e}^{-\mathrm{i}\omega_{nk}\left(t-t'\right)}, \tag{27b}$$

where T_n is the temperature of the nth bath [24].

The total SK action thus has two quartic terms, the influence phase displayed in equation (22) that stems from integrating out the bosonic environment, and the last term on the RHS of equation (21a) that stems from the Heisenberg spin-spin exchange interaction. These quartic terms can both be decoupled through the Hubbard–Stratonovich transformation [139], yielding the modified total action

$$S = \int_{\mathcal{C}}\mathrm{d}t\left[-\sum_{n}\varphi_n^{\mathrm{T}}\left(\frac{\mathrm{i}}{2}K^0\partial_t + \tilde{H}_n\right)\varphi_n + \frac{1}{4}\int_{\mathcal{C}}\mathrm{d}t'\sum_{\alpha n}\frac{\lambda^{\alpha}_n(t)\,\lambda^{\alpha}_n(t')}{\Xi^{\alpha}_n(t,t')} + \frac{1}{4}\sum\Lambda^{\alpha}_n\left[J^{-1}\right]^{\alpha\beta}_{nn'}\Lambda^{\beta}_{n'}\right]. \tag{28}$$

Here, the Hubbard–Stratonovich fields λ^{α}_n and Λ^{α}_n mediate the nonlocal-in-time spin-bath and the spin-spin interactions, respectively, and $\tilde{H}_n = \frac{1}{4}\sum_{\alpha}(h^{\alpha}+\lambda^{\alpha}_n+\Lambda^{\alpha}_n)K^{\alpha}$ is the effective Hamiltonian.

Nonequilibrium connected EVs can be obtained from the functional derivatives of the generating functional

$$W[J,K] = -\mathrm{i}\ln\int\mathcal{D}\Phi\,\exp\left(iS[\Phi] + \mathrm{i}\int_{\mathcal{C}}\mathrm{d}tJ(t)\,\Phi(t)\int_{\mathcal{C}}\mathrm{d}t\mathrm{d}t'\,K(t,t')\,\Phi(t)\,\Phi(t')\right), \tag{29}$$

where $\mathcal{D}\Phi$ indicates functional integration over all possible configurations of six-component field $\Phi = (\varphi,\lambda,\Lambda)^{\mathrm{T}}$, and J and K are one- and two-particle sources [23, 56], respectively. However, in practice this is a difficult calculation that requires perturbative approximation of the influence phase in equation (22), except for very simple environments [29]. Thus, it is more convenient to work with the Legendre transform of the functional $W[J,K]$ with respect to both arguments,

$$\Gamma\left[\bar{\Phi},G\right] = W[J,K] - \int_{\mathcal{C}}\mathrm{d}tJ(t)\,\bar{\Phi}(t) - \int_{\mathcal{C}}\mathrm{d}t\mathrm{d}t'\,K(t,t')\left(G(t',t) - \mathrm{i}\bar{\Phi}(t')\,\bar{\Phi}(t)\right), \tag{30}$$

known as the 2PI effective action [20, 22, 23]. Here, $\bar{\Phi}$ and G are the one- and two-particle connected EVs generated by $W[J,K]$. That is, $\bar{\Phi}$ is the EV and G is the connected GF of the fields. It is advantageous to work with $\Gamma[\bar{\Phi},G]$ instead of $W[J,K]$ because it produces EVs via a comparatively simpler variational approach, i.e. the full nonequilibrium EVs satisfy the saddle-point equations $\delta\Gamma/\delta\bar{\Phi} = 0$ and $\delta\Gamma/\delta G = 0$. Such variational calculations for real fields can be performed on the expansion [23, 60]

$$\Gamma\left[\bar{\Phi},G\right] = S\left[\bar{\Phi}\right] + \frac{\mathrm{i}}{2}\mathrm{Tr}\ln G^{-1} + \frac{\mathrm{i}}{2}\mathrm{Tr}\left[G_0^{-1}\left[\bar{\Phi}\right]G\right] - \mathrm{i}\Gamma_2, \tag{31}$$

where a constant term has been ignored; the trace is taken over all possible indices and times; $G_0^{-1} = \delta^2 S/\delta\bar{\Phi}\delta\bar{\Phi}$ is the inverse of the noninteracting GF including one-loop or mean-field corrections; and Γ_2 contains all 2PI vacuum Feynman diagrams. The 2PI diagrams contain two or more loops in which edges represent the full nonequilibrium GF G and vertices correspond to interactions contained in the action S, with possible insertions of the EV of the field $\bar{\Phi}$. Let us recall that 2PI diagrams are those that cannot be separated by cutting two edges or fewer, and vacuum diagrams have no external edges [23]. Since the diagrammatic expansion contained in Γ_2 is a functional of the *full interacting* nonequilibrium GF, each diagram within the 2PI effective action formalism effectively sums an infinite number of Feynman diagrams of particular topology with bare edges [58]. This can unravel effects that are *non-perturbative* [61, 62], which would otherwise be unattainable when using standard perturbative expansion in the coupling constant [136, 140, 141].

The spin-to-Schwinger-boson mapping implies that any EV containing an odd number of Schwinger bosons vanishes for physical states. In particular, $\bar{\varphi} = 0$ and $\langle\varphi(t)\lambda(t')\rangle = \langle\varphi(t)\lambda(t')\rangle = 0$. Additionally, $\langle\lambda(t)\Lambda(t')\rangle = 0$ due to the absence of terms coupling λ and Λ in the action of equation (28). Therefore, each diagram in the 2PI expansion is made up of vertices

Table 1. Summary of the key quantities of the SKFT+2PI framework for open quantum spin systems that appear in the equations of motion, equations (34) and (37), with their respective symbols, definitions, and labels. All indices are shown explicitly, such as $a,b=1\ldots4$, $\alpha,\beta=x,y,z$, and $n=1\ldots N_S$.

Symbol	Definition	Name	Symbol	Definition	Name
$\Xi_n^\alpha(t,t')$	$\sum_k (g_{nk}^\alpha)^2 B_{nk}^\alpha(t-t')$	Bath kernel	$\bar{\lambda}_n^\alpha(t)$	$\langle\lambda_n^\alpha(t)\rangle$	EV of the bath field
$J_{nn'}^{\alpha\beta}$		Heisenberg coupling	$\bar{\Lambda}_n^\alpha(t)$	$\langle\Lambda_n^\alpha(t)\rangle$	EV of the mean-field
$g_n^{ab}(t,t')$	$-\mathrm{i}\langle\varphi_n^b(t')\varphi_n^a(t)\rangle$	GF of the Schwinger bosons	$\Sigma_n^{ab}(t,t')$	$2\delta\Gamma_2/\delta g$	SE of the Schwinger bosons
$D_n^\alpha(t,t')$	$-\mathrm{i}\langle\lambda_n^\alpha(t')\lambda_n^\alpha(t)\rangle+\mathrm{i}\bar{\lambda}_n^\alpha(t)\bar{\lambda}_n^\beta(t')$	Bath propagator	$\Pi_n^\alpha(t,t')$	$2\delta\Gamma_2/\delta D$	SE of the bath
$M_{nn'}^{\alpha\beta}(t,t')$	$-\mathrm{i}\langle\Lambda_{n'}^\alpha(t')\Lambda_n^\beta(t)\rangle+\mathrm{i}\bar{\Lambda}_n^\alpha(t)\bar{\Lambda}_n^\beta(t')$	Mean-field propagator	$\Omega_n^{\alpha\beta}$	$2\delta\Gamma_2/\delta M$	SE of the mean-field
$\check{M}_{nn'}^{\alpha\beta}(t,t')$	equation (36)	Mean-field propagator			
$\tilde{H}_n^{ab}$	$\frac{1}{4}\sum_\alpha(h^\alpha+\lambda_n^\alpha+\Lambda_n^\alpha)K_{ab}^\alpha$	Effective Hamiltonian	K_{ab}^α	equation (20)	Spin matrices for real fields

(32)

where, within a particular diagram, solid lines correspond to the GF of the Schwinger bosons $\mathrm{i}g_{nn'}^{ab}(t,t')=\langle\varphi_n^a(t)\varphi_{n'}^b(t')\rangle$; dashed lines to the propagator $\mathrm{i}D_n^\alpha=\langle\lambda_n^\alpha(t)\lambda_n^\alpha(t')\rangle$; and wavy lines to the propagator $\mathrm{i}M_{nn'}^{\alpha\beta}=\left\langle\Lambda_n^\alpha(t)\Lambda_{n'}^\beta(t')\right\rangle$. Table 1 summarizes our nomenclature for all non-vanishing EVs and other relevant quantities.

Handling the infinite number of diagrams contained within Γ_2 in equation (31) requires a *controlled approximation* scheme. We adopt the scheme used in [56], where diagrams are truncated based on powers of the inverse of the number of Schwinger bosons $1/N$, which has been previously used to capture relevant features of closed quantum systems [53, 55, 56, 134, 142–144]. We emphasize that $N=2$ flavors of Schwinger bosons, which translate into an $O(4)$ theory, have been shown to already be remarkably close to the large-N limit in spite of our $N=2$ not being as large as typically invoked in elementary particle physics [61, 134]. The scaling with $1/N$ of a particular diagram is set by the number of closed loops of solid lines, and the number of dashed and wavy lines. Closed loops of solid lines scale $\sim N$ due to corresponding to traces over the space of Schwinger bosons. To determine the scaling of dashed (wavy) lines, we consider that all terms in the action of equation (28) are relevant in the large-N limit on the proviso that the bath kernel and the Heisenberg coupling constant scale as $\Xi\sim J\sim 1/N$ because the fields λ and Λ do not scale with N themselves. Then, the equations of motion equations (34*c*) and (34*b*), in which $D\sim\Xi$ and $M\sim J$, imply that dashed (wavy) lines scale $\sim 1/N$. Thus, the 2PI diagrams that scale with the lowest power of $1/N$ are the two-loop ones:

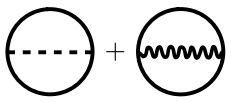

(33)

At this order of truncation, the equations of motion for the EVs of the fields and the connected nonequilibrium GFs, as obtained from the expansion of the 2PI action in equation (31) via variational principle, are given by

$$\partial_t g_n(t,t') = \mathrm{i}K^0\delta_{tt'} + 2\mathrm{i}K^0\tilde{H}_n(t)\,g_n(t,t') + \mathrm{i}K^0\int_{\mathcal{C}}\mathrm{d}t_1\,\Sigma_n(t,t_1)\,g_n(t_1,t')\,, \tag{34a}$$

$$M(t,t') = 2J\delta_{tt'} + 2\int_{\mathcal{C}}\mathrm{d}t_1\,J\Omega(t,t_1)\,M(t_1,t')\,, \tag{34b}$$

$$D_n^\alpha(t,t') = 2\Xi_n^\alpha(t,t') + 2\iint_{\mathcal{C}}\mathrm{d}t_1\mathrm{d}t_2\,\Xi_n^\alpha(t,t_1)\,\Pi_n^\alpha(t_1,t_2)\,D_n^\alpha(t_2,t')\,, \tag{34c}$$

$$\bar{\Lambda}(t) = \frac{\mathrm{i}}{2}J\mathrm{Tr}_S[Kg(t,t)]\,, \tag{34d}$$

$$\bar{\lambda}_n^{\alpha}(t) = \frac{\mathrm{i}}{2}\int_{\mathcal{C}} \mathrm{d}t'\, \Xi_n^{\alpha}(t,t')\,\mathrm{Tr}_S\left[K^{\alpha} g_n(t',t')\right]. \tag{34e}$$

We remind the reader that definitions for all quantities in these equations are provided in table 1. Here, matrix multiplication is assumed for indices not shown; Tr_S traces over the space of Schwinger bosons; $\delta_{tt'}$ is the contour Dirac delta function [22]; integrals are over the SK closed contour $\mathcal{C}$; and $\Pi = 2\delta\Gamma_2/\delta D$, $\Omega = 2\delta\Gamma_2/\delta M$, and $\Sigma = 2\delta\Gamma_2/\delta g$ are the self-energies (SEs) derived through functional differentiation of the 2PI vacuum diagrams. The diagrams considered within our $1/N$ expansion (equation (33)) yield expressions for the SEs

$$\Pi_n^{\alpha}(t,t') = \frac{\mathrm{i}}{8}\mathrm{Tr}_S\left[K^{\alpha} g_n(t,t') K^{\alpha} g_n^{\mathrm{T}}(t,t')\right], \tag{35a}$$

$$\Omega_n^{\alpha\beta}(t,t') = \frac{\mathrm{i}}{8}\mathrm{Tr}_S\left[K^{\alpha} g_n(t,t') K^{\beta} g_n^{\mathrm{T}}(t,t')\right], \tag{35b}$$

$$\Sigma^{ab}(t,t') = \frac{\mathrm{i}}{4}\sum_{\alpha} K^{\alpha} g_n(t,t') K^{\alpha} D_n^{\alpha}(t,t') + \frac{\mathrm{i}}{4}\sum_{\alpha\beta} K^{\alpha} g_n(t,t') K^{\beta} M_{nn}^{\alpha\beta}(t,t'). \tag{35c}$$

Although the GF of the Schwinger bosons $g_{nn'}$ can in principle be nonlocal in space, such as in spin systems with fractional excitations [131, 145], the separable initial spin states we consider in this work imply $g_{nn'} = g_n\delta_{nn'}$ at all times, and, therefore $\Sigma_{nn'}, \Omega_{nn'}, \Pi_{nn'} \propto \delta_{nn'}$. The self-consistency [58] built into 2PI resummation and the SEs evades [54] the so-called secularity problem for expansion in terms of the free Keldysh GFs, where elapsed time appearing next to the coupling constant makes the effective coupling arbitrarily large at late times. The same self-consistency ensures that all conservation laws are satisfied in spite of truncating the diagrammatic expansion [135].

Equations (34) and (35), which utilize integrals over the SK contour $\mathcal{C}$, can be transformed to contain real-time integrals by decomposing all GFs and SEs into their Keldysh and spectral components according to equation (26). In addition to the M^K and M^s components, the propagator $M(t,t')$ has a time-local part proportional to $\delta_{tt'}$ (equation (34b)). The time-local part can be extracted by defining $\check{M}(t,t')$ such that

$$M(t,t') = 2J\delta_{tt'} + J\check{M}(t,t')J. \tag{36}$$

Assuming that there is no single-ion anisotropy, i.e. $J_{nn}^{\alpha\beta} = 0$, no other GFs or SEs have a time-local component. Therefore, the system of equations of motion that produce the real-time dynamics of the system are given by

$$\partial_t g_n^K(t,t') = 2\mathrm{i}K^0\tilde{H}_n(t) g_n^K(t,t') + \mathrm{i}K^0\int_0^t \mathrm{d}t_1\, \Sigma_n^s(t,t_1) g_n^K(t_1,t') - \mathrm{i}K^0\int_0^{t'} \mathrm{d}t_1\, \Sigma_n^K(t,t_1) g_n^s(t_1,t'), \tag{37a}$$

$$\partial_t g_n^s(t,t') = 2\mathrm{i}K^0\tilde{H}_n(t) g_n^s(t,t') + \mathrm{i}K^0\int_{t'}^t \mathrm{d}t_1\, \Sigma_n^s(t,t_1) g_n^s(t_1,t'), \tag{37b}$$

$$\check{M}^K(t,t') = 4\Omega^K(t,t') + 2\int_0^t \mathrm{d}t_1\, \Omega^s(t,t_1) J\check{M}^K(t_1,t') - 2\int_0^{t'} \mathrm{d}t_1\, \Omega^K(t,t_1) J\check{M}^s(t_1,t') \tag{37c}$$

$$\check{M}^s(t,t') = 4\Omega^s(t,t') + 2\int_{t'}^t \mathrm{d}t_1\, \Omega^s(t,t_1) J\check{M}^s(t_1,t') \tag{37d}$$

$$\begin{aligned} D_n^{\alpha K}(t,t') = {} & 2\Xi_n^{\alpha K}(t,t') + 2\int_0^t\int_0^{t_1} \mathrm{d}t_1\mathrm{d}t_2\, \Xi_n^{\alpha s}(t,t_1)\Pi_n^{\alpha s}(t_1,t_2) D_n^{\alpha K}(t_2,t') \\ & + 2\int_0^{t'}\int_0^{t_1} \mathrm{d}t_1\mathrm{d}t_2\, \Xi_n^{\alpha K}(t,t_2)\Pi_n^{\alpha s}(t_2,t_1) D_n^{\alpha s}(t_1,t') \\ & - 2\int_0^t\int_0^{t'} \mathrm{d}t_1\mathrm{d}t_2\, \Xi_n^{\alpha s}(t,t_1)\Pi_n^{\alpha K}(t_1,t_2) D_n^{\alpha s}(t_2,t'), \end{aligned} \tag{37e}$$

$$D_n^{\alpha s}(t,t') = 2\Xi_n^{\alpha s}(t,t') + 2\int_{t'}^t\int_{t'}^{t_1} \mathrm{d}t_1\mathrm{d}t_2\, \Xi_n^{\alpha s}(t,t_1)\Pi_n^{\alpha s}(t_1,t_2) D_n^{\alpha s}(t_2,t'), \tag{37f}$$

$$\begin{aligned} \Sigma_n^K(t,t') = {} & \frac{\mathrm{i}}{8}\sum_{\alpha}\left\{K^{\alpha} g_n^K(t,t') K^{\alpha} D_n^{\alpha K}(t,t') + K^{\alpha} g_n^s(t,t') K^{\alpha} D_n^{\alpha s}(t,t')\right\} \\ & + \frac{\mathrm{i}}{8}\sum_{\alpha\beta}\left\{K^{\alpha} g_n^K(t,t') K^{\beta}\left[J\check{M}^K(t,t')J\right]_{nn}^{\alpha\beta} + K^{\alpha} g_n^s(t,t') K^{\beta}\left[J\check{M}^s(t,t')J\right]_{nn}^{\alpha\beta}\right\}, \end{aligned} \tag{37g}$$

$$\Sigma_n^s(t,t') = \frac{\mathrm{i}}{8}\sum_{\alpha}\left\{K^\alpha g_n^K(t,t')K^\alpha D_n^{\alpha s}(t,t') + K^\alpha g_n^s(t,t')K^\alpha D_n^{\alpha K}(t,t')\right\} \tag{37h}$$

$$+\frac{\mathrm{i}}{8}\sum_{\alpha\beta}\left\{K^\alpha g_n^K(t,t')K^\beta\left[J\check{M}^s(t,t')J\right]_{nn}^{\alpha\beta} + K^\alpha g_n^s(t,t')K^\beta\left[J\check{M}^K(t,t')J\right]_{nn}^{\alpha\beta}\right\},$$

$$\Omega_n^{\alpha\beta K}(t,t') = \frac{\mathrm{i}}{16}\mathrm{Tr}_S\left[K^\alpha g_n^K(t,t')K^\beta g_n^{KT}(t,t') + K^\alpha g_n^s(t,t')K^\beta g_n^{sT}(t,t')\right], \tag{37i}$$

$$\Omega_n^{\alpha\beta s}(t,t') = \frac{\mathrm{i}}{8}\mathrm{Tr}_S\left[K^\alpha g_n^K(t,t')K^\beta g_n^{sT}(t,t')\right], \tag{37j}$$

$$\Pi_n^{\alpha K}(t,t') = \frac{\mathrm{i}}{16}\mathrm{Tr}_S\left[K^\alpha g_n^K(t,t')K^\alpha g_n^{KT}(t,t') + K^\alpha g_n^s(t,t')K^\alpha g_n^{sT}(t,t')\right], \tag{37k}$$

$$\Pi_n^{\alpha s}(t,t') = \frac{\mathrm{i}}{8}\mathrm{Tr}_S\left[K^\alpha g_n^K(t,t')K^\alpha g_n^{sT}(t,t')\right], \tag{37l}$$

$$\bar{\Lambda}_n^\alpha(t) = \frac{\mathrm{i}}{4}\sum_{\beta n'} J_{nn'}^{\alpha\beta}\mathrm{Tr}_S\left[K^\beta g_{n'}^K(t,t)\right], \tag{37m}$$

$$\bar{\lambda}_n^\alpha(t) = \frac{\mathrm{i}}{4}\int_0^t \mathrm{d}t_1\,\Xi_n^{\alpha s}(t,t_1)\,\mathrm{Tr}_S\left[K^\alpha g_n^K(t_1,t_1)\right], \tag{37n}$$

which are obtained from combining the equations of motion for the GFs on the Keldysh contour (equation (34)) with the expressions for the SEs (equation (35)) and using the decomposition of equation (26) and (36) to extract the Keldysh and spectral components.

4.1. Spin EVs and two-spin correlators from SKFT+2PI

The dynamics of spin EVs is obtained from the SKFT+2PI equations of motion from

$$\langle\hat{s}_n^\alpha\rangle(t) = \frac{\mathrm{i}}{8}\mathrm{Tr}_S\left[g_n^K(t,t)K^\alpha\right]. \tag{38}$$

As such, the EV of the Hubbard–Stratonovich fields can be expressed as

$$\bar{\Lambda}_n^\alpha(t) = 2\sum_{\beta n'} J_{nn'}^{\alpha\beta}\langle\hat{s}_n^\alpha\rangle(t), \tag{39a}$$

$$\bar{\lambda}_n^\alpha(t) = \int_0^t \mathrm{d}t_1\,\Xi_n^{\alpha s}(t,t_1)\,\langle\hat{s}_n^\alpha\rangle(t_1). \tag{39b}$$

The RHS of equation (39*a*) is proportional to the magnetic mean field that spin n is subject to due to being coupled to other spins via Heisenberg exchange. The dynamics of the propagator of the mean field, $\mathrm{i}M_{nn'}^{\alpha\beta}(t,t') = \left\langle\Lambda_n^\alpha(t)\Lambda_{n'}^\beta(t')\right\rangle$, includes all fluctuations of Λ_n^α. Similarly, the RHS of equation (39*b*) is an average over all past spin states weighed by the spectral component of the bath kernel $\Xi_n^{\alpha s}$, highlighting the generally non-Markovian nature of the dynamics.

The two-spin connected correlator functions $\left\langle s_n^\alpha(t)s_{n'}^\beta(t')\right\rangle$ in the SKFT+2PI approach are obtained from the connected generating functional

$$W[\eta] = -\mathrm{i}\ln\int\mathcal{D}\Phi\,\exp\left(\mathrm{i}S[\Phi] + \frac{\mathrm{i}}{4}\int_{\mathcal{C}}\mathrm{d}t\sum_{n\alpha}\eta_n^\alpha\varphi_n^{\mathrm{T}}K^\alpha\varphi_n\right) \tag{40}$$

via functional derivative with respect to the source field η_n^α in the limit where η_n^α vanishes, i.e.

$$\left\langle s_n^\alpha(t)\,s_{n'}^\beta(t')\right\rangle = -\mathrm{i}\frac{\delta^2 W[\eta]}{\delta\eta_n^\alpha(t)\,\delta\eta_{n'}^\beta(t')}\bigg|_{\eta=0}. \tag{41}$$

The source term can be absorbed into the effective Hamiltonian, so that $\tilde{H}_n[\eta] = \frac{1}{4}\sum_\alpha(h^\alpha + \lambda_n^\alpha + \Lambda_n^\alpha + \eta_n^\alpha)K^\alpha$. Since the functional integral is over all configurations of the fields, it is invariant under the constant shift $\Lambda \to \Lambda - \eta$. Such shift produces an action identical to the one in equation (28), except that the last term on the RHS becomes

$$\frac{1}{4}\int_{\mathcal{C}}\mathrm{d}t\sum(\Lambda_n^\alpha - \eta_n^\alpha)\left[J^{-1}\right]_{nn'}^{\alpha\beta}\left(\Lambda_{n'}^\beta - \eta_n^\alpha\right). \tag{42}$$

Now taking the functional derivative with respect to source η generates EVs of the mean field Λ. It turns out that

$$\left\langle s_n^\alpha(t)\, s_{n'}^\beta(t')\right\rangle = \frac{\mathrm{i}}{4}\check{M}_{nn'}^{\alpha\beta}(t,t')\,, \tag{43}$$

where we used equation (36) to isolate the time-local part of the mean field propagator. Instead of shifting the mean field Λ_n^α, the bath field λ_n^α can also be shifted, potentially leading to an expression for the two-spin correlator in terms of the bath propagator D_n^α. However, such approach is made difficult by requiring to carefully invert convolutions with the bath kernel Ξ_n^α on the SK contour. Thus, we compute two-spin correlators exclusively via equation (43).

In single-spin systems, such as the spin-boson model (equation (2)), there is no mean field propagator. Still, the two-spin correlator $\langle s^\alpha(t)s^\beta(t')\rangle$ at the same site but for different times and spin components can be obtained by introducing a replica spin and bath with identical initial states. By weakly coupling the spin and its replica ferromagnetically, the two-spin correlator between the spin and its replica mimics the original same-site two-spin correlator.

4.2. Numerical implementation of SKFT+2PI equations

The equations of motion produced by SKFT+2PI form an integro-differential system of the Volterra type [146, 147] that must be integrated carefully due to the self-consistent interdependence between 14 functions. For this purpose, we discretize both time arguments t and t', so that all functions of two times can be considered matrices in these two arguments. The Keldysh and spectral components are symmetric and antisymmetric, respectively, under transposition and exchange of the two time arguments, i.e.

$$O^{K/s}(t,t') = \pm\left(O^{K/s}\right)^{\mathrm{T}}(t',t)\,. \tag{44}$$

Therefore, it suffices to compute and store all quantities at times $t' \leq t$.

For the numerical integration of the integro-differential system in equation (37), we implement a predictor-corrector algorithm which consists of two stages. In the first (predictor) stage, the RHSs of equations (37*a*) and (37*b*) are computed using all known quantities for all t' and the current t. The results are used to predict the GFs of the Schwinger bosons at the next time $t+h$, i.e. $\tilde{g}_n^{K/s}(t+h,t') = g_n^{K/s}(t,t') + h\partial_t g_n^F(t,t')$ where h is the time step, for all discrete t'. Predicting the diagonal time step $\tilde{g}_n^K(t+h,t+h)$ requires the derivative with respect to the second time argument, $\partial_{t'} g_n^K(t,t')$, obtained from the transpose of equation (37*a*) and the symmetry properties of the nonequilibrium GFs in equation (44). The time-diagonal of $g_n^s(t,t) = -\mathrm{i}\langle[\varphi_n^b(t), \varphi_n^a(t)]\rangle = \mathrm{i}K^0$ is fixed by the equal-time commutation relations of the Schwinger bosons. With the predicted values for the GFs of the Schwinger bosons $\tilde{g}_n^{K/s}(t+h,t')$, the value of all the other functions at the next time step can be predicted in the order shown in figure 3. All integrals appearing on the RHSs of equations (37) are computed with the trapezoid method, although higher performance could be achieved by implementing recently developed integration schemes based on tensor trains [148, 149].

In the second (corrector) stage of the predictor-corrector algorithm, the predicted quantities are used to recompute the RHSs of equations (37*a*) and (37*b*). The new value for the GFs of the Schwinger bosons is then obtained from averaging the RHSs of equations (37*a*) and (37*b*) obtained in the prediction and correction stages, i.e.

$$g_n^{K/s}(t+h,t') = g_n^{K/s}(t,t') + \frac{h}{2}\left[\partial_t g_n^{K/s}(t,t') + \partial_t \tilde{g}_n^{K/s}(t+h,t')\right]. \tag{45}$$

Using the corrected $g_n^{K/s}(t+h,t')$, all other quantities are recalculated following the same order as in the predictor stage (figure 3). It is possible to repeat the corrector stage iteratively to improve accuracy of the algorithm, but we find that a single run is enough to achieve convergence for the studied models. We also choose small enough time steps so that further decrease does not result in appreciable changes to the results. Typically, this means employing time steps $h = 0.1/\Delta$, but shorter ones are required as the system-bath coupling is increased, down to $h = 0.03/\Delta$ in the ultrastrong coupling regime. Additional details of this type of predictor-corrector scheme can be found in [56].

In order to estimate the numerical cost of solving the equations of motion produced by SKFT+2PI, we evolved one closed system and two open systems using our implementation of the predictor-corrector algorithm. For the closed system, we choose an AF spin chain subjected to a transverse field along the x-axis (equation (4*a*)). For the open systems, we evolve the spin-boson model (equation (2)) and the

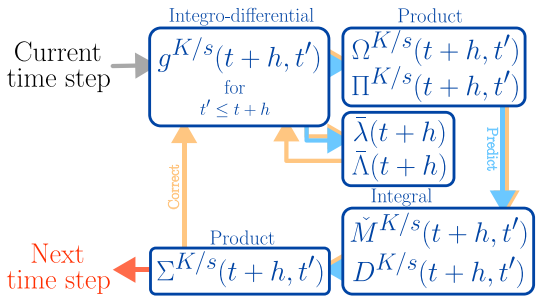

Figure 3. Flowchart of the predictor-corrector algorithm used in the numerical integration of SKFT+2PI-derived coupled equations (37*a*)–(37*n*). The type of equation used at each step (integro-differential, integral, or generalized matrix product) is indicated in dark blue. All sub- and super-scripts are omitted for simplicity (see table 1 for their detailed notation). Functions at time t are used as an input to the prediction stage (light blue arrows), in which all functions are computed at the next time step $t+h$ for all $t' \leqslant t+h$, starting with the Keldysh and spectral components of the GFs of the Schwinger bosons $g^{K/s}$. The results of the prediction stage are used to correct $g^{K/s}$, as well as subsequent functions, by repeating the cycle of the self-consistent loop (orange lines). The results of the correction stage are saved as the values for the next time step.

spin-chain-boson-model with an independent bosonic bath for each spin (equation (4), but the first sum in equation (4*b*) is over $n = 1, 2, \ldots, N_S$). As a function of the number of spins N_S, the elapsed time for both closed and open systems scales as $\propto N_S^3$. This is due to the largest matrix being the propagator $\check{M}^{\alpha\beta}_{nn'}(t,t')$ (table 1), which can be reshaped into a $3N_S \times 3N_S$ matrix. Concomitantly, the total memory allocated scales as $\propto N_S^2$. On the other hand, as a function of the number of time steps N_t, both the elapsed time and the memory scale as $\propto N_t^3$ for the closed system, and as $\propto N_t^4$ for the open systems. This is because evolving functions of two times t, t' for N_t time steps requires computing and storing such functions at $\propto N_t^2$ pairs of times. Moreover, computing each one of those values requires performing single (for the closed system) or double (for the open systems) time integrals, which scale as $\propto N_t$ and $\propto N_t^2$, respectively, therefore producing the observed scaling.

4.3. Initial conditions and the Schwinger boson constraint

Initial conditions must be given to begin the predictor-corrector algorithm. Within the SKFT+2PI approach, initial states must be described by a Gaussian density operator [22, 55, 56], i.e. only the EVs and the connected nonequilibrium GFs of the fields are nonzero. In this work, we consider separable initial states described by a density operator that is a tensor product

$$\hat{\rho}\,(t=0) = \bigotimes_{\nu} \hat{\rho}^B_\nu \bigotimes_{n} \hat{\rho}^S_n. \tag{46}$$

Here, $\hat{\rho}^B_\nu$ is the thermal density operator of bosonic bath ν at temperature T_ν, and $\hat{\rho}^S_n$ is a Gaussian density operator for spin n. In our numerical implementation of the SKFT+2PI equations, these initial conditions are achieved by setting the bath propagator as $D^{K/s}(0,0) = 2\Xi^{K/s}(0,0)$, as well as the GFs of the Schwinger bosons as $ig^K_n(0,0) = \sum_\alpha 2K^\alpha \langle \hat{s}^\alpha_n(0)\rangle + S + \frac{1}{2}$ and $g^s_n = \mathrm{i}K^0$.

Due to the symmetries of the SK action (equation (28)), the total number of bosons per site is conserved [56]. Therefore, if the initial conditions satisfy the Schwinger boson constraint in equation (17), it will also be satisfied at *all* later times. This is in contrast to the usage of Schwinger bosons in imaginary time calculations, which require enforcing the constraint via Lagrange multipliers [129–131]. The Gaussian initial conditions we employ enforce that the EV of the constraint

$$\left\langle \hat{a}^{(1)\dagger}_n \hat{a}^{(1)}_n + \hat{a}^{(2)\dagger}_n \hat{a}^{(2)}_n \right\rangle = 2S, \tag{47}$$

holds at all times. Deviations from this equality are typically less than 10^{-14} in our numerical implementation (inset of figure 4(a)). However, the original Schwinger boson constraint (equation (17)) relates *operators*, which implies infinite additional constraints in terms of EVs, namely,

$$\left\langle \left(\hat{a}^{(1)\dagger}_n \hat{a}^{(1)}_n + \hat{a}^{(2)\dagger}_n \hat{a}^{(2)}_n \right)^2 \right\rangle = (2S)^2, \tag{48a}$$

$$\left\langle \left(\hat{a}^{(1)\dagger}_n \hat{a}^{(1)}_n + \hat{a}^{(2)\dagger}_n \hat{a}^{(2)}_n \right)^3 \right\rangle = (2S)^3, \tag{48b}$$

$$\vdots$$

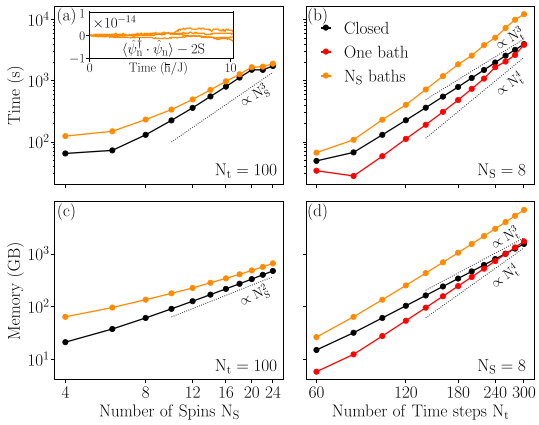

Figure 4. (a), (b) Elapsed time and (c), (d) memory consumed by our numerical implementation of the predictor-corrector algorithm for solving the SKFT+2PI equations (37*a*)–((37*n*) as a function of the number of spins N_S (left column of panels) or the number of time steps N_t (right column of panels). The black lines are for a closed AF spin chain in a transverse magnetic field (equation (4*a*)); the red ones are for the spin-boson model (equation (2)); and the orange ones are for the spin-chain-boson model with N_S baths (equation (4)) where *each* spin couples to three independent baths. The inset in panel (a) shows numerical deviations from the EV of the Schwinger boson constraint (equation (48)) in the case of a spin-chain-boson model with $N_S = 4$.

Because these higher-order EVs are zero for an initial Gaussian density operator, the constraints in equation (48) are not satisfied at any time $t \geq 0$. Thus, artifactual virtual processes outside the physical finite-size Hilbert space of spins can contribute (see section 5.2) to the discrepancy between SKFT+2PI and numerically (quasi)exact benchmark results. It is worth noting that problems posed by the Gaussian initial state are unrelated to the truncation of the 2PI effective action. In fact, *if* one were able to provide the full correct initial state, all Schwinger boson constraints derived from the operator identity in equation (17) would be satisfied despite truncating the diagrammatic expansion. However, usage of arbitrary initial states for time evolution via SKFT is an unsolved problem, despite many proposed remedies [150–154].

5. Results and discussion

5.1. Dynamics of semiclassical spins

To understand the physical meaning of SKFT+2PI equations (37), we warm up in this section by discussing semiclassical spin dynamics [155–157], which is easier to decipher than fully quantum dynamics of spin-boson (section 5.2) and spin-chain-boson (section 5.3) models. Such dynamics is obtained from SKFT+2PI by neglecting even the $1/N^0$ contributions to the 2PI effective action, i.e. $\Gamma_2 \equiv 0$ in equation (31). Under this approximation, all SEs vanish, and equations (37) of motion decouple. Using equation (38) for the EVs of the spins and equation (37*a*) for the evolution of the Keldysh GF of the Schwinger bosons g^K yields

$$\partial_t \langle s_n^\alpha \rangle (t) = \sum_{\beta\gamma} \epsilon_{\alpha\beta\gamma} \left(h_n^\beta + \lambda_n^\beta + \Lambda_n^\beta \right) \langle s_n^\alpha \rangle (t) , \tag{49}$$

where $\epsilon_{\alpha\beta\gamma}$ is the Levi–Civita symbol. By defining the vector of spin EVs, $\mathbf{S}_n \equiv (\langle s_n^x \rangle , \langle s_n^y \rangle , \langle s_n^z \rangle)$, and by using equations (39) for the fields λ_n^β and Λ_n^β, the time evolution $\mathbf{S}_n(t)$ is given by

$$\partial_t \mathbf{S}_n (t) = \mathbf{h}_n^{\text{eff}} \times \mathbf{S}_n (t) - \mathbf{S}_n (t) \times \int_0^t \mathrm{d}t' \, \eta_n (t, t') \cdot \mathbf{S}_n (t') , \tag{50}$$

where the effective magnetic field is $h_n^{\alpha\,\text{eff}} = h_n^\alpha + \Lambda_n^\alpha$. Equation (50) is of the Landau–Lifshitz type [158], but it is 'extended' by having non-Markovian kernel $\eta_n^{\alpha\beta}(t, t') = \delta^{\alpha\beta} \Xi_n^{\alpha s}(t, t')$ due to effects of the bosonic baths. Similar equations have been recently derived [155–157, 159–161], including via the minimization of the SK action with respect to quantum fluctuations [155, 156]. Thus, our SKFT+2PI formalism further justifies such derivations by explaining that they utilize *only* the first three terms on the RHS of equation (31) containing tree-level or classical (1st term on the RHS of equation (31)) and one-loop or semiclassical (2nd and 3rd terms on the RHS of equation (31)) diagrams of the 2PI effective action [162]. If multiple spins are allowed to couple to a single bath, the non-Markovian kernel in equation (50), besides being nonlocal in time, also becomes nonlocal in space [155, 161].

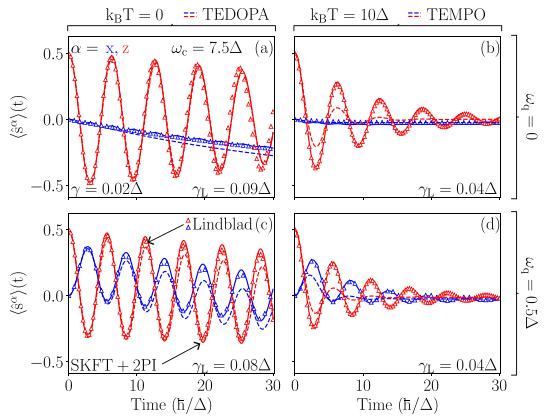

Figure 5. Time dependence of spin expectation values $\langle \hat{s}^{\alpha} \rangle$ of the spin-boson model (equation (2)) computed from our SKFT+2PI (solid lines) approach vs. standard Lindblad QME (triangles) or TN methods (dashed lines) with bath cutoff frequency $\omega_c = 7.5\Delta$ in the *weak* system-bath coupling regime, $\gamma \ll \Delta$, where the system dynamics is expected [7] to be *Markovian* [88, 89] for the chosen Ohmic bath [$s = 1$ in equation (3)]. Panels in different columns and rows use different values of temperature T and two-level splitting ω_q, respectively. For $k_B T = 0$, the chosen TN method is TEDOPA, while for $k_B T = 10\Delta$, we use TEMPO (see sections 3.2 and 5 for details). The SKFT+2PI and TN-computed benchmark results follow each other closely for the chosen $\gamma = 0.02\Delta$, while the system-bath coupling in equations (14) and (15) for the Lindblad QME, γ_L, must be adjusted by increasing it to match the other two calculations (this points to artifacts of the Lindblad QME derived [1] for the spin-boson model).

The spectral component of the bath kernel $\Xi_n^{\alpha s}(t,t')$, which yields the non-Markovian kernel within equation (50), is computed for the spectral density in equation (3) for arbitrary parameter s via equations (23) and (27) to give

$$\Xi_n^{\alpha s}(t,t') = -\frac{\gamma_n^{\alpha}\omega_c^2}{\pi}\frac{\Gamma(1+s)\sin\left[(1+s)\tan^{-1}(\omega_c\tau)\right]}{\left[1+(\omega_c\tau)^2\right)\right]^{(1+s)/2}}. \tag{51}$$

Here, $\tau \equiv t - t'$, and $\Gamma(x)$ is the Gamma function. The slow algebraic decay of $\Xi_n^{\alpha s}(\tau)$ is linked to non-analyticities of the spectral density [163], namely, the second derivative of $\mathcal{J}(\omega)$ in equation (3) is not defined at $\omega = 0$. Such power law decay of the bath kernel means that the contribution of states in the far past to the dynamics of open quantum systems can persist beyond other relevant time scales. For instance, even if the system-bath coupling γ is small, a low cutoff frequency ω_c ensures that the power law tails of the bath are relevant, and the dynamics *remains non-Markovian*.

Nevertheless, Markovian dynamics of the extended LLG equation (50) can be recovered in the limit $\omega_c \to \infty$ of an Ohmic bath $s = 1$ [79, 156] for which the bath kernel becomes local in time $\Xi_n^{\alpha s}(t,t') = \gamma_n^{\alpha}\partial_t\delta(t-t')$. In this limit, the non-Markovian equation (50) simplifies into

$$\partial_t \mathbf{S}_n(t) = \mathbf{h}_n^{\text{eff}} \times \mathbf{S}_n(t) - \gamma_n \mathbf{S}_n(t) \times \partial_t \mathbf{S}_n(t), \tag{52}$$

where we also assume isotropic spin-bath couplings, for simplicity. Equation (52) is the standard Landau–Lifshitz–Gilbert equation [158], in which damping term (second on the RHS) is in the Gilbert form [164]. Considering the parameter $s \neq 1$ transmutes the time derivative in the damping term of equation (52) into a fractional derivative [156].

5.2. Dynamics of the spin-boson model

In this section, we present dynamics of spin EV in the spin-boson model (equation (2)) using the Ohmic ($s = 1$ in equation (3)) and sub-Ohmic baths ($s = 0.5$ in equation (3)). We start with the analysis of the Markovian regime in figure 5 for which we employ small $\gamma = 0.02\Delta$ and high $\omega_c = 7.5\Delta$ to ensure entering such a regime [88]. The Markovian nature of the results in figure 5 is signified by the irreversible decay of purity (orange solid line in figure 6) of the mixed quantum state of spin $S = 1/2$. Since the spin density operator $\hat{\rho}^S$ for $S = 1/2$ and the Bloch vector $\mathbf{P} = (P^x, P^y, P^z)$ are in one-to-one correspondence [30]

$$\hat{\rho} = \frac{1}{2}\left(\hat{I} + 2\sum_{\alpha} P^{\alpha}\hat{s}^{\alpha}\right), \tag{53}$$

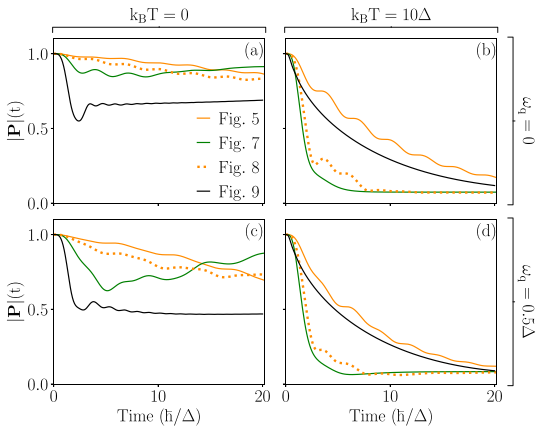

Figure 6. Time dependence of purity $|\mathbf{P}| = 2\sqrt{\sum_\alpha \langle \hat{s}_\alpha \rangle^2}$ of mixed quantum state of spin $S = 1/2$ from SKFT+2PI-computed curves in figures 5–9. Orange, green, and black solid lines are for the case of an Ohmic bath (figures 5, 7 and 9), while orange dotted line is for the case of a sub-Ohmic bath (figure 8).

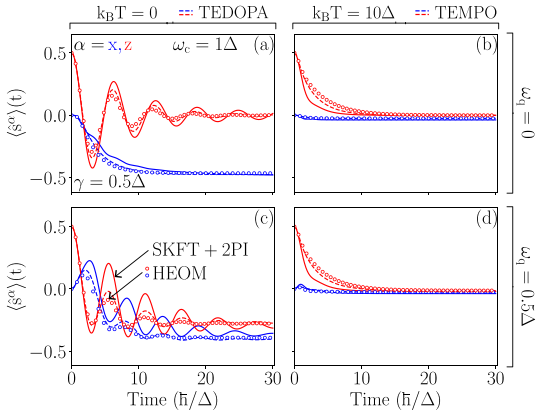

Figure 7. The same information as in figure 5, but for bath cutoff frequency $\omega_c = 1\Delta$ and in the *strong* system-bath coupling regime, $\gamma = 0.5\Delta$, where the system dynamics is expected to be *non-Markovian* [88, 89] for the chosen [7] Ohmic bath [$s = 1$ in equation (3)]. Different columns and rows of panels use different values of temperature T and two-level splitting ω_q (equation (2)), respectively. Note that standard HEOM calculations [65] cannot be conducted at $k_BT = 0$ temperature, so in the left column of panels we use higher temperature $k_BT = 0.1\Delta$ in HEOM calculations instead of $k_BT = 0$ [as marked on the top of panel (a)] employed in SKFT+2PI and TN-based calculations.

where $\hat{I}$ is the unit operator in the spin space, we use $|\mathbf{P}|$ as a measure of the state purity. The standard purity $\mathrm{Tr}\hat{\rho}^2$ is a function of $|\mathbf{P}|$, where $|\mathbf{P}| = 1$ signifies a fully coherent or pure quantum state of spin $S = 1/2$, while $0 \leq |\mathbf{P}| < 1$ denotes mixed quantum states. In figure 5, we find excellent agreement between SKFT+2PI (solid lines) and Lindblad-QME-computed results (triangles). However, such a match is *ensured only* by adjusting the system-bath coupling in the Lindblad QME, thereby pointing to an artifact of the standard equation for the spin-boson model [1]. This is because our SKFT+2PI results independently and closely match the results of TN calculations (dashed lines in figures 5 and 7) employing the same γ. Our TN calculations for the $k_BT = 0$ case used TEDOPA [66–68], whereas for the higher temperature $k_BT = 10\Delta$ we switched to TEMPO [40, 69]. Beyond the Markovian regime, the Lindblad QME cannot capture the memory effects of the bath, which can cause the revival of quantum properties. Such revival is exemplified by the purity $|\mathbf{P}|$ of the mixed quantum state of spin initially decaying in figures 6(a) and (c), as the signature of decoherence [31], but later increasing towards $|\mathbf{P}| = 1$ of the pure state at $t = 0$ as the signature of recoherence [3].

In the non-Markovian regime of figure 7, we replace benchmarking via the Lindblad QME with HEOM and TN-based benchmarks. The non-Markovian regime is induced by using a strong system-bath coupling $\gamma = 0.5\Delta$ and low cutoff frequency $\omega_c = \Delta$, while keeping the Ohmic bath as in figure 5. We find that, for zero temperature, the TEDOPA results (dashed lines in figures 7(a) and (c)) follow closely those from HEOM (circles in figure 7), on the proviso that we use slightly higher temperature $k_BT = 0.1\Delta$ in the HEOM calculations. The necessity for such an ad hoc fixing of standard HEOM calculations stems from their *inability* to handle $k_BT = 0$ limit [85, 86, 90]. The spin EV computed by

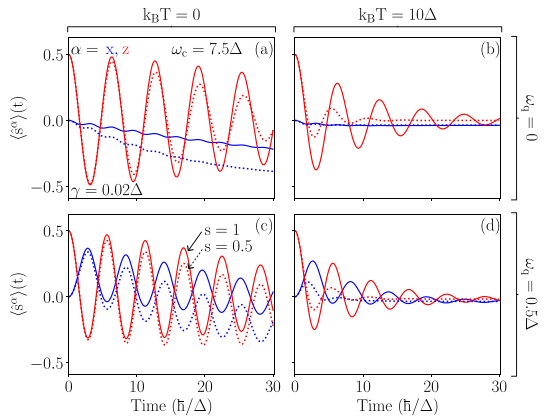

Figure 8. Time dependence of spin expectation values $\langle \hat{s}^\alpha \rangle$ computed from SKFT+2PI for bosonic bath with Ohmic (solid lines) or sub-Ohmic (dotted lines) spectral density, i.e. $s = 1$ or $s = 0.5$ in equation (3), respectively. Other parameters are the same as in the weak system-bath coupling regime of figure 5. Note that solid lines are identical to solid lines in figure 5, which are plotted here for easy comparison.

SKFT+2PI is capable of tracking both benchmark results, but it appears as if its damping is slightly smaller (compare solid lines from SKFT+2PI to circles from HEOM and dashed lines from TEDOPA calculations in figure 7(c)).

Furthermore, figure 8 demonstrates the ability of our SKFT+2PI formalism to treat various other parameter regimes of the system and bath, such as the case of zero temperature and sub-Ohmic bath that is considered particularly challenging [74, 78–81, 85]. For this purpose, we compute from SKFT+2PI the spin EV for a sub-Ohmic bath ($s = 0.5$ in equation (3)) while using the same values of other parameters as in the weak system-bath coupling regime of figure 5 for the sake of comparing Ohmic vs. sub-Ohmic cases. The results in figure 8 show faster decrease of the spin EV when the bath is sub-Ohmic. However, the purity in the sub-Ohmic case (orange dotted line in figure 6) *does not* decay monotonically as in the case of the Markovian regime for the Ohmic bath (orange solid line in figure 6). Instead, at zero temperature it saturates at a finite value, akin to the Ohmic non-Markovian case (green and black lines in figure 6 obtained using SKFT+2PI from figures 7 and 9). Moreover, at high temperature, the purity of spin state in the sub-Ohmic regime closely resembles the time evolution of it in the strong system-bath coupling (i.e. non-Markovian) regime, except for small revivals (orange dotted curve in figures 6(b) and (d)) at intermediate time scales. Thus, figure 6 illustrates the difficulties [74, 78–81, 85] posed by the sub-Ohmic case because of the skew towards low bath frequencies (figure 1(a)) which enhances the memory effects of the bath. These features make it possible for the non-Markovian regime to emerge *despite* weak system-bath coupling.

Finally, we examine the non-Markovian regime brought by ultrastrong system-bath coupling $\gamma = 4\Delta$ (figure 9), while keeping the remaining parameters the same as in figure 7. At zero temperature of this regime, the spin-boson transition to a localized phase occurs [165, 166]. It is characterized by long-range correlations in time and $\langle \hat{s}^z \rangle (t)$ saturating at a finite value despite the presence of the dissipative environment and regardless of two-level splitting ω_q. Such saturation is observed in the stationary state of the spin EV obtained with both TEDOPA and our SKFT+2PI, demonstrating the ability of the latter to capture highly non-perturbative effects. The quantum phase transition can be further probed by computing the order parameter m^2 [165, 166], given by the time integral

$$m^2 = \int \mathrm{d}t \mathrm{i} C^{zz,K}(t,0)\,, \tag{54}$$

of the Keldysh component of the connected two-spin correlator $C^{\alpha\beta}_{nn'}(t,t') = 4\mathrm{i}\left\langle s^\alpha_n(t) s^\beta_{n'}(t') \right\rangle$, as obtained via equation (26). Such an order parameter is zero in the delocalized phase (figures 5, 7 and 8), but it abruptly acquires a finite value in the localized phase (figure 9). The two-spin correlator extracted from SKFT+2PI on the delocalized side of the transition oscillates as a function of time (orange line in figure 10(b)), whereas it is almost always positive on the localized side (green line in figure 10(b)). Integrating the two-spin correlator over time for different system-bath couplings, the non-thermal critical coupling [167] is found to be $\gamma_c \approx \Delta$ in figure 10. In this calculation, we use $\omega_q = 0$, $s = 0.5$ and $\omega_c = \Delta$.

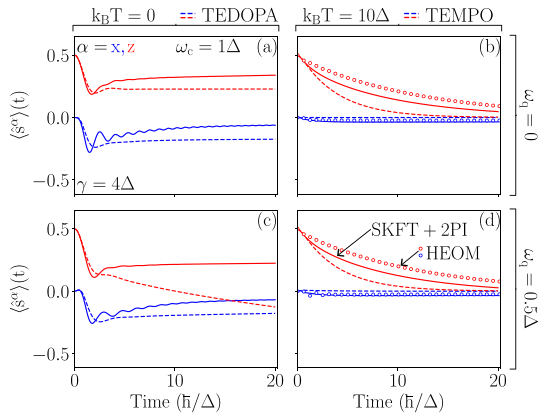

Figure 9. The same information as in figure 7, but for bath cutoff frequency $\omega_c = 1\Delta$ and in the *ultrastrong* system-bath coupling regime, $\gamma = 4\Delta$, where the system dynamics is expected to be *highly non-Markovian* [88, 89] for the chosen [7] Ohmic bath ($s = 1$ in equation (3)). The ultrastrong system-bath coupling induces localization [165, 166] of the spin for $k_BT = 0$, i.e. $\langle \hat{s}^z \rangle (t)$ plateaus at a finite noninteger value. This non-perturbative behavior of a plateau reached in the long-time limit is captured by SKFT+2PI (solid lines), but the asymptotic value defining the plateau differs from the TN-computed benchmark (dashed lines) at low temperatures.

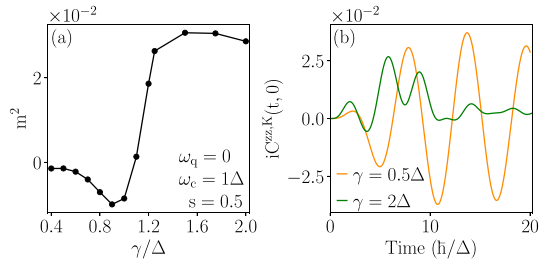

Figure 10. (a) Order parameter (equation (54)) of the quantum phase transition [165, 166] of the spin-boson model as a function of the system-bath coupling constant γ. The transition is signified by a kink at the critical coupling $\gamma_c \approx \Delta$ [166]. (b) Multitime two-spin correlator, at time t and the initial time $t = 0$, for γ values in the delocalized (orange line) and localized phase (green lines), respectively.

Nevertheless, in the localized phase, SKFT+2PI predicts an incorrect long-time limit of the spin EV, especially for $\omega_q = 0.5\Delta$ (figure 9(c)). We believe that such discrepancy stems from the initial conditions being restricted to a Gaussian density operator, since, in the localized phase, properties of the initial state are not erased by the bath. Such memory effects make the stationary spin EV particularly sensitive to any non-Gaussian initial correlations. These are not captured by SKFT+2PI, but are well described by TEDOPA. On the other hand, SKFT+2PI performs much better for ultrastrong coupling at high temperatures (figures 9(b) and (d)) than TN-based calculations like TEMPO, where the latter struggles to converge in the same regime. In fact, in this regime, SKFT+2PI results match the HEOM benchmark better than TEMPO results. Let us re-emphasize that the standard version of HEOM cannot [85, 86, 90] handle zero temperature $k_BT = 0$, which is essential for the transition to the localized phase, and so HEOM results are omitted from figures 9(a) and (c).

5.3. Dynamics of the spin-chain-boson model

The spin-chain-boson model (figure 1(b)) employed in this section is described by the Hamiltonian in equation (4) using $N_S = 4$ quantum spins $S = 1/2$ with AF exchange coupling between the nearest neighbors $J^{\alpha\beta}_{n,n+1} = J^{\alpha\beta}_{n,n-1} = J\delta^{\alpha\beta}$. A set of three independent bosonic baths, one for each spin component, is coupled to each end of the chain, as needed for spins interacting with phonons in three-dimensional magnetic materials [33, 34]. The temperature of the three baths coupled to spin $n = 1$ is $k_BT_1 = 5J$, while the temperature of the three baths coupled to spin $n = 4$ is $k_BT_4 = 0$. All other parameters are the same for simplicity, and the external magnetic field is chosen as $\mathbf{h} = (J, 0, 0)$.

The dynamics of the spin $n = 4$ EV is shown in figure 11(b). Note that in this case we could not produce any benchmarks from either HEOM (because of too many spins) or from TN calculations (because of difficulties found in the packages [40] we employ when trying to handle multiple baths). The complexity of physics generated by multiple baths has been noticed previously [32] even in the case of single spin. We start from the Néel ket $|\uparrow\downarrow\uparrow\downarrow\rangle$ in which $\langle \hat{s}^z_1 \rangle = \langle \hat{s}^z_3 \rangle = 1$ and $\langle \hat{s}^z_2 \rangle = \langle \hat{s}^z_4 \rangle = -1$. The fact that

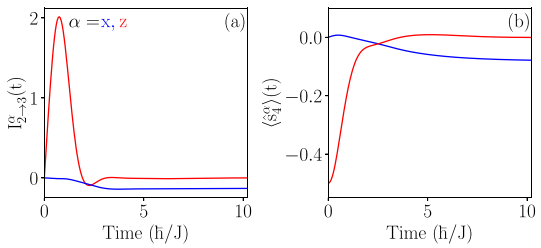

Figure 11. SKFT+2PI-computed time dependence of the Cartesian components of: (a) the bond spin current (equation (55)) between sites $n = 2$ and $n' = 3$; and (b) EV of spin at the right edge ($n = 4$). The spin-chain-boson model considered in this calculation is AF, composed of $N_S = 4$ spins and driven by temperature gradient, $k_B T_1 = 5J$ and $k_B T_4 = 0$, as illustrated in figure 1(b). Other parameters of the six baths employed are $\omega_c = 3J$ and $\gamma^\alpha = 0.5J$.

dynamics of spin EV in figure 11(b), as well as of EVs of other three spins not shown, tend to small values $2|\langle \hat{\mathbf{s}}_n \rangle| \ll 1$ signifies nonzero entanglement of a mixed quantum state. The entanglement can remain nonzero, despite the presence of a dissipative environment, due to the non-Markovian regime of open quantum system dynamics [117].

The open AF quantum spin chain with different temperatures of the baths connected at its boundaries [168] will also exhibit nonequilibrium spin and heat currents [169, 170]. Since the total heat current requires three-spin correlators [169, 170], which are inaccessible from our current implementation of our SKFT+2PI formalism, we compute only spin current as an illustration. The α-component of the bond spin current between two spins n, n' is expressed as [169]

$$I^{\alpha}_{n\to n'}(t) = -8J \sum_{\beta\gamma} \epsilon_{\alpha\beta\gamma} \left\langle s^{\alpha}_{n}(t)\, s^{\beta}_{n'}(t) \right\rangle^{K}, \tag{55}$$

using the Keldysh component of two-spin correlators (equation (43) at equal times). The time dependence of the bond spin currents $I^{\alpha}_{n\to n'}$, out of which we plot only $I^{x}_{2\to 3}$ and $I^{z}_{2\to 3}$ in figure 11, is driven by the temperature difference between the baths at two different edges. The bond current $I^{x}_{2\to 3}$ has a finite value in the steady state because of the externally applied magnetic field $\mathbf{h}$ along the x-axis. On the other hand, $I^{z}_{2\to 3}$ is transiently nonzero but vanishes in the long-time limit. Transient oscillation of the currents within the spin chain can be long-lived due to finite-size effects. However, the decay of such oscillations in figure 11(e) is accelerated by virtual processes outside of the physical Hilbert space. These processes can be caused by artifacts of resumming infinitely-many Feynman diagrams [171] or by neglected initial non-Gaussian correlations [172].

5.4. Dynamics of closed quantum spins

Since our SKFT+2PI also describes the limiting case of a closed system of quantum spins, we also benchmark such calculations for the sake of completeness. Such closed quantum system dynamics is obtained by considering only the second diagram in equation (33) due to spin-spin interaction. We recall that the time evolution of a closed system of quantum spins has already been studied by different flavors of SKFT+2PI formalism in [56] and [55], whose purpose is to enable handling of hundreds of spins in three spatial dimensions. In contrast, TN methods, which can handle large numbers of spins in low dimensions, fail in higher dimensions due to increased entanglement [52, 174, 175]. However, examples studied in [56] and [55] were not benchmarked against numerically exact dynamics, which can always be computed for sufficiently small systems. Therefore, in figure 12, we plot the time evolution of EV of a selected spin within a 3×3 cluster of FM (figure 12(a)) or AF (figure 12(b)) coupled quantum spins, as computed via SKFT+2PI (solid lines) or exact diagonalization for time-dependent systems [173] (dashed lines). The comparison of trajectories in figure 12 shows that SKFT+2PI for closed quantum spin systems fails after a relatively short evolution time, appearing as if it is damped and, therefore, converging to a stationary state *despite the absence* of a dissipative environment. This failure of previously developed SKFT+2PI for closed quantum systems [55, 56] is due to virtual processes outside the physical Hilbert space, as has also been pointed out in other problems involving fermionic [171] and bosonic [53] degrees of freedom. For fermionic systems, these virtual processes are thought to be found within the resummation of infinitely many Feynman diagrams, since diagrams of high enough order describe processes involving more fermions than are allowed by a finite system [171]. Although such artificial processes would cancel in an exact theory, this is not necessarily the case when only diagrams of particular topology are summed to infinite order [171]. However, in unconstrained

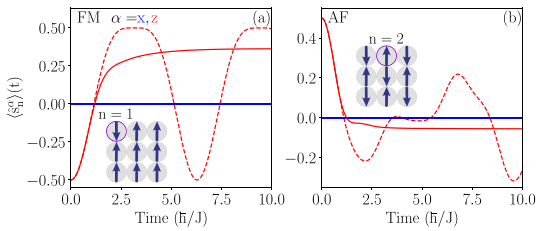

Figure 12. Time dependence of EV of a single spin $\langle \hat{s}_n^\alpha \rangle (t)$, whose selection is marked in the insets, within a closed 3×3 lattice of two-dimensional (a) FM or (b) AF cluster. The initial states are illustrated in the insets of each panel. The solid lines are computed by SKFT+2PI of [56] for closed quantum spin systems, while the dashed lines are obtained by exact diagonalization for time-dependent systems [173].

bosonic systems, the equivalent high-order processes are within the infinite-dimensional Hilbert space. In such a case, reasons for the failure of SKFT+2PI for closed systems are less clear, although it has been conjectured to also be due to neglected diagrams [53]. For constrained bosonic systems, such as the Schwinger bosons onto which we map spin operators, we believe that neglected non-Gaussian correlations of the initial state significantly contribute to the discrepancy between SKFT+2PI and the benchmarks in figure 12, as discussed in section 4.3. The artifactual stationary state produced by SKFT+2PI in figure 12 is determined by the total energy and magnetization of the initial state, since these are conserved by the symmetries of the action in equation (28). Thus, in the FM system with all-but-one spins initially pointing up (illustrated in the inset of figure 12(a)), the SKFT+2PI-obtained stationary state reflects these conservation laws as it converges to uniform but not saturated magnetization $\langle \hat{s}_n^z(t \to \infty) \rangle < 1$. Similarly, in the AF system initially (illustrated in the inset of figure 12(b)) in the *unentangled* Neél state, a nonzero initial magnetization (due to an odd number of spins) is conserved into the stationary limit.

6. Conclusions and outlook

In conclusion, we construct a promising field-theoretic approach to driven-dissipative many-body systems, as one of the most challenging unsolved problems in quantum physics [176]. This approach can tackle various dynamical regimes and system geometries or dimensionalities [45, 51]. In contrast, previously developed methods, when applied to the spin-boson model as a standard testbed [70], require changing the method (such as HEOM [65] vs. different flavors of TN approaches [40, 41]) depending on the chosen parameters of the model. Furthermore, we also demonstrate how our SKFT+2PI framework can handle *many* interacting quantum spins with *noncommuting* couplings to *multiple* [32–34] baths generating the *non-Markovian* regime of the dynamics of spins. The complexity of such a setup (figure 1(b)) causes impediments even for very recent TN methods developed [39] for this frontier problem due to transient entanglement barrier [114–116], even in the presence of a dissipative environment [117]. In addition, our SKFT+2PI framework can handle arbitrary spin value S in arbitrary geometry [52] or spatial dimensionality [45, 51], which benefits quantum spintronics [46–50] and quantum magnonics [51], where the spin value $S \geq 1/2$; as well as quantum computing [45] where $S = 1/2$ for qubits [35, 36] and $S > 1/2$ for qudits [177].

The ability of our SKFT+2PI framework to closely track numerical (quasi)exact results from TN methods applied to the spin-boson model demonstrates that our field-theoretic approach is *non-perturbative* in the system-bath coupling. This achievement can be traced back to the usage of 2PI resummation of a class of infinitely many Feynman diagrams generated by the $1/N$ expansion, instead of conventional perturbative expansion in the system-bath coupling. Nevertheless, full understanding of how our 2PI and $1/N$ resum conventional perturbative expansion in the system-bath coupling constant to achieve non-perturbative regimes is lacking. It could be further clarified by constructing the associated resurgent transseries in the coupling constant [62] and comparing it with our expansion. In addition, our SKFT+2PI offers a *single unified framework* that can handle arbitrary temperature, cutoff frequency, and spectral content of the bosonic baths (i.e. Ohmic vs. sub-Ohmic vs. super-Ohmic), or exchange interaction between many spins. Unlike widely used QMEs for open quantum system dynamics [1], where only the reduced density operator is accessible as a function of single time, *both* our SKFT+2PI framework and TN methods [40, 41] make possible computation of multitime two-spin correlators. For

example, using such correlators, we can obtain the order parameter (figure 10) of delocalized-localized quantum phase transition in the spin-boson model or nonequilibrium spin current (figure 11) in the spin-chain-boson model biased by a temperature gradient. This can be of great interest to modeling experiments on quantum magnets, such as quantum spin liquids [145], where thermal transport is one of the major tools [178].

The numerical cost of solving integro-differential equations (37*a*)–(37*n*) produced by SKFT+2PI formalism for open quantum spin systems is cubic-scaling in the number of spins N_S of arbitrary value S, as well as quartic-scaling in the number of time steps N_t. The latter computational complexity could, in principle, be lowered [146–149, 179, 180] by optimizing numerics. One of the main avenues for lowering p in the scaling $\propto N_t^p$ is by introducing a memory cut, which consists of neglecting contributions to the dynamics from states before a fixed cutoff time. However, SEs and kernels related to the environment surrounding open systems may decay algebraically in time [163], rather than exponentially as in closed systems, for which memory cuts have already been implemented [56, 146, 147]. This is precisely the case for a bosonic bath with any s parameter in equation (3). As such, implementing memory cuts in open quantum systems requires additional efforts beyond those of [56, 146, 147].

Finally, we point out that the occasional discrepancies between the SKFT+2PI framework and numerically (quasi)exact benchmarks, particularly conspicuous in figure 9 for ultrastrong system-bath coupling, largely stem from the truncation (equation 33) of the diagrammatic series, which may neglect high-energy excitations [53] or include unphysical virtual processes [171]. Our benchmarking efforts suggest that neglected initial higher-order correlations [172] may also significantly contribute to such discrepancies, but this issue is much less explored in the literature. This is because non-Gaussian initial correlations are required to constrain the dynamics of the infinite-dimensional Schwinger bosons to the finite physical subspace. Including the environment in our formulation of SKFT+2PI for *open* quantum spin systems alleviates the issues posed by the neglected non-Gaussian correlations by effectively erasing the initial conditions at longer times. However, when the system transitions into a localized phase, memory of the initial conditions is retained well into the stationary regime, so deviations from numerically (quasi)exact benchmarks emerge again (figures 9(a) and (c)). Therefore, finding a general and practical solution to the fundamental problem [150] of how to include *arbitrary* non-Gaussian initial states into SKFT could further improve the capabilities of our approach.

Data availability statement

The data that support the findings of this study are available upon reasonable request from the authors.

Acknowledgments

We are grateful to L E Herrera Rodríguez for technical help regarding the intricacies of HEOM calculations and to J Varela-Manjarrés for helpful discussions. F R -O, F G -G and B K N were supported by the U S National Science Foundation (NSF) under Grant No. DMR-2500816. P P was partially supported by the U S Army Research Office under Grant No. W911NF-22-2-0234. S R C gratefully acknowledges financial support from the UK's Engineering and Physical Sciences Research Council (EPSRC) under Grant No. EP/T028424/1.

ORCID iDs

Felipe Reyes-Osorio 0000-0002-6399-2524
Federico García-Gaitán 0009-0007-8090-8316
Stephen R Clark 0000-0002-2072-7499
Branislav K Nikolić 0000-0002-5793-7764

References

[1] Breuer H-P and Petruccione F 2007 *The Theory of Open Quantum Systems* (Oxford University Press)
[2] Reimer V, Wegewijs M R, Nestmann K and Pletyukhov M 2019 Five approaches to exact open-system dynamics: Complete positivity, divisibility and time-dependent observables *J. Chem. Phys.* **151** 044101
[3] Breuer H-P, Laine E-M, Piilo J and Vacchini B 2016 Colloquium: Non-Markovian dynamics in open quantum systems *Rev. Mod. Phys.* **88** 021002
[4] de Vega I and Alonso D 2017 Dynamics of non-Markovian open quantum systems *Rev. Mod. Phys.* **89** 015001
[5] Fazio R, Keeling J, Mazza L and Schirò M 2025 Many-body open quantum systems *SciPost Phys. Lect. Notes* 99

[6] Lindblad G 1976 On the generators of quantum dynamical semigroups *Commun. Math. Phys.* **48** 119
[7] Nathan F and Rudner M S 2020 universal Lindblad equation for open quantum systems *Phys. Rev. B* **102** 115109
[8] Rivas A, Huelga S F and Plenio M B 2014 Quantum non-Markovianity: characterization, quantification and detection *Rep. Prog. Phys.* **77** 094001
[9] Nakajima S 1958 On quantum theory of transport phenomena: steady diffusion *Prog. Theor. Phys.* **20** 948
[10] Zwanzig R 1960 Ensemble method in the theory of irreversibility *J. Chem. Phys.* **33** 1338
[11] Chruściński D and Kossakowski A 2010 Non-Markovian quantum dynamics: local versus nonlocal *Phys. Rev. Lett.* **104** 070406
[12] Nestmann K and Wegewijs M R 2021 General connection between time-local and time-nonlocal perturbation expansions *Phys. Rev. B* **104** 155407
[13] Nestmann K, Bruch V and Wegewijs M R 2021 How quantum evolution with memory is generated in a time-local way *Phys. Rev. X* **11** 021041
[14] Anto-Sztrikacs N and Segal D 2021 Capturing non-Markovian dynamics with the reaction coordinate method *Phys. Rev. A* **104** 052617
[15] Prosen T 2008 Third quantization: a general method to solve master equations for quadratic open Fermi systems *New J. Phys.* **10** 043026
[16] Barthel T and Zhang Y 2022 Solving quasi-free and quadratic Lindblad master equations for open fermionic and bosonic systems *J. Stat. Mech* 113101
[17] McDonald A and Clerk A A 2023 Third quantization of open quantum systems: Dissipative symmetries and connections to phase-space and Keldysh field-theory formulations *Phys. Rev. Res.* **5** 033107
[18] Sieberer L M, Buchhold M and Diehl S 2016 Keldysh field theory for driven open quantum systems *Rep. Prog. Phys.* **79** 096001
[19] Thompson F and Kamenev A 2023 Field theory of many-body Lindbladian dynamics *Ann. Phys., NY* **455** 169385
[20] Rammer J 2007 *Quantum Field Theory of Non-Equilibrium States* (Cambridge University Press)
[21] Calzetta E A and Hu B-L B 2008 *Nonequilibrium Quantum Field Theory* (Cambridge University Press)
[22] Berges J 2015 Nonequilibrium quantum fields: from cold atoms to cosmology (arXiv:1503.02907)
[23] Gelis F 2019 *Quantum Field Theory: From Basics to Modern Topics* (Cambridge University Press)
[24] Kamenev A 2023 *Field Theory of Non-Equilibrium Systems* (Cambridge University Press)
[25] Stefanucci G 2024 Kadanoff-Baym equations for interacting systems with dissipative Lindbladian dynamics *Phys. Rev. Lett.* **133** 066901
[26] Maghrebi M F and Gorshkov A V 2016 Nonequilibrium many-body steady states via Keldysh formalism *Phys. Rev. B* **93** 014307
[27] Müller C and Stace T M 2017 Deriving Lindblad master equations with Keldysh diagrams: correlated gain and loss in higher order perturbation theory *Phys. Rev. A* **95** 013847
[28] Leggett A J, Chakravarty S, Dorsey A T, Fisher M P A, Garg A and Zwerger W 1987 Dynamics of the dissipative two-state system *Rev. Mod. Phys.* **59** 1
[29] Feynman R and Vernon F 1963 The theory of a general quantum system interacting with a linear dissipative system *Ann. Phys.* **24** 118
[30] Ballentine L E 2014 *Quantum Mechanics: A Modern Development* (World Scientific)
[31] Joos E, Zeh H D, Kiefer C, Giulini D, Kupsch J and Stamatescu I-O 2003 *Decoherence and the Appearance of a Classical World in Quantum Theory* (Springer)
[32] Bruognolo B, Weichselbaum A, Guo C, von Delft J, Schneider I and Vojta M 2014 Two-bath spin-boson model: phase diagram and critical properties *Phys. Rev. B* **90** 245130
[33] Nemati S, Henkel C and Anders J 2022 Coupling function from bath density of states *Europhys. Lett.* **139** 36002
[34] Hogg C R, Cerisola F, Cresser J D, Horsley S A R and Anders J 2024 Enhanced entanglement in multi-bath spin-boson models *Quantum* **8** 1357
[35] Gulácsi B and Burkard G 2023 Signatures of non-Markovianity of a superconducting qubit *Phys. Rev. B* **107** 174511
[36] Rossini M, Maile D, Ankerhold J and Donvil B I C 2023 Single-qubit error mitigation by simulating non-Markovian dynamics *Phys. Rev. Lett.* **131** 110603
[37] Koch C P 2016 Controlling open quantum systems: tools, achievements and limitations *J. Phys.: Condens. Matter* **28** 213001
[38] Harrington P M, Mueller E J and Murch K W 2022 Engineered dissipation for quantum information science *Nat. Rev. Phys.* **4** 660
[39] Fux G E, Kilda D, Lovett B W and Keeling J 2023 Tensor network simulation of chains of non-Markovian open quantum systems *Phys. Rev. Res.* **5** 033078
[40] Fux G E *et al* 2024 OQuPy: a Python package to efficiently simulate non-Markovian open quantum systems with process tensors *J. Chem. Phys.* **161** 124108
[41] Cygorek M and Gauger E M 2024 ACE: a general-purpose non-Markovian open quantum systems simulation toolkit based on process tensors *J. Chem. Phys.* **161** 074111
[42] Sun Y, Wang G and Cai Z 2024 Simulation of spin chains with off-diagonal coupling using the inchworm method *J. Chem. Theory Comput.* **20** 9321
[43] Xu M, Stockburger J T and Ankerhold J 2024 Environment-mediated long-ranged correlations in many-body system *J. Chem. Phys.* **161** 124105
[44] Lindoy L P, Rodrigo-Albert D, Rath Y and Rungger I 2025 pyTTN: an open source toolbox for open and closed system quantum dynamics simulations using tree tensor networks (arXiv:2503.15460)
[45] Rosenberg D *et al* 2017 3D integrated superconducting qubits *npj Quantum Inf.* **3** 42
[46] Petrović M D, Mondal P, Feiguin A E, Plecháč P and Nikolić B K 2021 Spintronics meets density matrix renormalization group: quantum spin-torque-driven nonclassical magnetization reversal and dynamical buildup of long-range entanglement *Phys. Rev. X* **11** 021062
[47] Suresh A, Soares R D, Mondal P, Pires J P S, Lopes J M V P, Ferreira A, Feiguin A E, Plecháč P and Nikolić B K 2024 Electron-mediated entanglement of two distant macroscopic ferromagnets within a nonequilibrium spintronic device *Phys. Rev. A* **109** 022414
[48] Kovarik S, Schlitz R, Vishwakarma A, Ruckert D, Gambardella P and Stepanow S 2024 Spin torque–driven electron paramagnetic resonance of a single spin in a pentacene molecule *Science* **384** 1368

[49] Choi D-J, Lorente N, Wiebe J, von Bergmann K, Otte A F and Heinrich A J 2019 *Colloquium*: atomic spin chains on surfaces *Rev. Mod. Phys.* **91** 041001
[50] Chen Y, Bae Y and Heinrich A J 2023 Harnessing the quantum behavior of spins on surfaces *Adv. Mater.* **35** 2107534
[51] Yuan H, Cao Y, Kamra A, Duine R A and Yan P 2022 Quantum magnonics: when magnon spintronics meets quantum information science *Phys. Rep.* **965** 1
[52] Patra S, Singh S and Orús R 2025 Projected entangled pair states with flexible geometry *Phys. Rev. Res.* **7** L012002
[53] Rey A M, Hu B L, Calzetta E, Roura A and Clark C W 2004 Nonequilibrium dynamics of optical-lattice-loaded Bose-Einstein-condensate atoms: Beyond the Hartree-Fock-Bogoliubov approximation *Phys. Rev. A* **69** 033610
[54] Borsányi S 2005 Nonequilibrium field theory from the 2PI effective action (arXiv:0512308)
[55] Babadi M, Demler E and Knap M 2015 Far-from-equilibrium field theory of many-body quantum spin systems: prethermalization and relaxation of spin spiral states in three dimensions *Phys. Rev. X* **5** 041005
[56] Schuckert A, Orioli A and Berges J 2018 Nonequilibrium quantum spin dynamics from two-particle irreducible functional integral techniques in the Schwinger boson representation *Phys. Rev. B* **98** 224304
[57] Hosseinabadi H, Chang D E and Marino J 2024 Far from equilibrium field theory for strongly coupled light and matter: dynamics of frustrated multimode cavity QED *Phys. Rev. Res.* **6** 043314
[58] Brown M and Whittingham I 2015 Two-particle irreducible effective actions versus resummation: analytic properties and self-consistency *Nucl. Phys. B* **900** 477
[59] Mera H, Pedersen T G and Nikolić B K 2016 Hypergeometric resummation of self-consistent sunset diagrams for steady-state electron-boson quantum many-body systems out of equilibrium *Phys. Rev. B* **94** 165429
[60] Cornwall J M, Jackiw R and Tomboulis E 1974 Effective action for composite operators *Phys. Rev. D* **10** 2428
[61] Mariño M 2015 *Instantons and Large N: An Introduction to Non-Perturbative Methods in Quantum Field Theory* (Cambridge University Press) (https://doi.org/10.1017/cbo9781107705968)
[62] Di Pietro L, Mari no M, Sberveglieri G and Serone M 2021 Resurgence and 1/N expansion in integrable field theories *J. High Energy Phys.* JHEP10(2021)166
[63] Aniceto I, Başar G and Schiappa R 2019 A primer on resurgent transseries and their asymptotics *Phys. Rep.* **809** 1
[64] Mera H, Pedersen T G and Nikolić B K 2018 Fast summation of divergent series and resurgent transseries from Meijer-*g* approximants *Phys. Rev. D* **97** 105027
[65] Tanimura Y 2020 Numerically exact approach to open quantum dynamics: the hierarchical equations of motion (HEOM) *J. Chem. Phys.* **153** 020901
[66] de Vega I and Ba nuls M-C 2015 Thermofield-based chain-mapping approach for open quantum systems *Phys. Rev. A* **92** 052116
[67] Chin A W, Rivas A, Huelga S F and Plenio M B 2010 Exact mapping between system-reservoir quantum models and semi-infinite discrete chains using orthogonal polynomials *J. Math. Phys.* **51** 092109
[68] Ye E and Chan G K-L 2021 Constructing tensor network influence functionals for general quantum dynamics *J. Chem. Phys.* **155** 044104
[69] Strathearn A, Kirton P, Kilda D, Keeling J and Lovett B W 2018 Efficient non-Markovian quantum dynamics using time-evolving matrix product operators *Nat. Commun.* **9** 3322
[70] Vilkoviskiy I and Abanin D A 2024 Bound on approximating non-Markovian dynamics by tensor networks in the time domain *Phys. Rev. B* **109** 205126
[71] Makri N 1995 Numerical path integral techniques for long time dynamics of quantum dissipative systems *J. Math. Phys.* **36** 2430
[72] Winter A, Rieger H, Vojta M and Bulla R 2009 Quantum phase transition in the sub-Ohmic spin-boson model: quantum Monte Carlo study with a continuous imaginary time cluster algorithm *Phys. Rev. Lett.* **102** 030601
[73] Wang H and Thoss M 2008 From coherent motion to localization: dynamics of the spin-boson model at zero temperature *New J. Phys.* **10** 115005
[74] Wang H and Thoss M 2010 From coherent motion to localization: II. dynamics of the spin-boson model with sub-Ohmic spectral density at zero temperature *Chem. Phys.* **370** 78
[75] Strathearn A, Lovett B W and Kirton P 2017 Efficient real-time path integrals for non-Markovian spin-boson models *New J. Phys.* **19** 093009
[76] Cygorek M, Cosacchi M, Vagov A, Axt V M, Lovett B W, Keeling J and Gauger E M 2022 Simulation of open quantum systems by automated compression of arbitrary environments *Nat. Phys.* **18** 662
[77] Weber M 2022 Quantum Monte Carlo simulation of spin-boson models using wormhole updates *Phys. Rev. B* **105** 165129
[78] Bulla R, Tong N-H and Vojta M 2003 Numerical renormalization group for bosonic systems and application to the sub-Ohmic spin-boson model *Phys. Rev. Lett.* **91** 170601
[79] Anders F B and Schiller A 2006 Spin precession and real-time dynamics in the Kondo model: time-dependent numerical renormalization-group study *Phys. Rev. B* **74** 245113
[80] Anders F B, Bulla R and Vojta M 2007 Equilibrium and nonequilibrium dynamics of the sub-Ohmic spin-boson model *Phys. Rev. Lett.* **98** 210402
[81] Vojta M 2012 Numerical renormalization group for the sub-Ohmic spin-boson model: a conspiracy of errors *Phys. Rev. B* **85** 115113
[82] Orth P P, Imambekov A and Le Hur K 2013 Nonperturbative stochastic method for driven spin-boson model *Phys. Rev. B* **87** 014305
[83] Scarlatella O and Schirò M 2024 Self-consistent dynamical maps for open quantum systems *SciPost Phys.* **16** 026
[84] Ivander F, Lindoy L P and Lee J 2024 Unified framework for open quantum dynamics with memory *Nat. Commun.* **15** 8087
[85] Xu M and Ankerhold J 2023 About the performance of perturbative treatments of the spin-boson dynamics within the hierarchical equations of motion approach *Eur. Phys. J. Spec. Top.* **232** 3209–17
[86] Xu M, Vadimov V, Krug M, Stockburger J T and Ankerhold J 2023 A universal framework for quantum dissipation: minimally extended state space and exact time-local dynamics (arXiv:2307.16790)
[87] Shibata F and Arimitsu T 1980 Expansion formulas in nonequilibrium statistical mechanics *J. Phys. Soc. Japan* **49** 891
[88] Clos G and Breuer H-P 2012 Quantification of memory effects in the spin-boson model *Phys. Rev. A* **86** 012115
[89] Wenderoth S, Breuer H-P and Thoss M 2021 Non-Markovian effects in the spin-boson model at zero temperature *Phys. Rev. A* **104** 012213

[90] Xu M, Yan Y, Shi Q, Ankerhold J and Stockburger J T 2022 Taming quantum noise for efficient low temperature simulations of open quantum systems *Phys. Rev. Lett.* **129** 230601
[91] Weber M, Luitz D J and Assaad F F 2022 Dissipation-induced order: the $s = 1/2$ quantum spin chain coupled to an Ohmic bath *Phys. Rev. Lett.* **129** 056402
[92] Yang K, Morampudi S C and Bergholtz E J 2021 Exceptional spin liquids from couplings to the environment *Phys. Rev. Lett.* **126** 077201
[93] Scheie A, Laurell P, Samarakoon A M, Lake B, Nagler S E, Granroth G E, Okamoto S, Alvarez G and Tennant D A 2021 Witnessing entanglement in quantum magnets using neutron scattering *Phys. Rev. B* **103** 224434
[94] Nuomin H, Song F-F, Zhang P and Beratan D N 2025 Correlated reaction coordinate motion produces nonadditive rate enhancement for electron and energy transfer in multiacceptor structures *J. Am. Chem. Soc.* **147** 26877
[95] Xu M, Song L, Song K and Shi Q 2017 Convergence of high order perturbative expansions in open system quantum dynamics *J. Chem. Phys.* **146** 064102
[96] Chen H-T, Cohen G and Reichman D R 2017 Inchworm Monte Carlo for exact non-adiabatic dynamics. I. theory and algorithms *J. Chem. Phys.* **146** 054105
[97] Chen H-T, Cohen G and Reichman D R 2017 Inchworm Monte Carlo for exact non-adiabatic dynamics. II. benchmarks and comparison with established methods *J. Chem. Phys.* **146** 054106
[98] Goulko O, Chen H-T, Goldstein M and Cohen G 2025 Transient dynamical phase diagram of the spin-boson model *Phys. Rev. Lett.* **134** 056502
[99] Nguyen H, Ng N, Lindoy L P, Park G, Millis A J, Kin-Lic Chan G and Reichman D R 2024 Correlation functions from tensor network influence functionals: the case of the spin-boson model *J. Chem. Phys.* **161** 104111
[100] Tanimura Y and Wolynes P G 1991 Quantum and classical Fokker-Planck equations for a Gaussian-Markovian noise bath *Phys. Rev. A* **43** 4131
[101] Huang Y-T, Kuo P-C, Lambert N, Cirio M, Cross S, Yang S-L, Nori F and Chen Y-N 2023 An efficient Julia framework for hierarchical equations of motion in open quantum systems *Commun. Phys.* **6** 313
[102] Meier C and Tannor D 1999 Non-Markovian evolution of the density operator in the presence of strong laser fields *J. Chem. Phys.* **111** 3365
[103] Lambert N, Raheja T, Cross S, Menczel P, Ahmed S, Pitchford A, Burgarth D and Nori F 2023 QuTiP-BoFiN: a bosonic and fermionic numerical hierarchical-equations-of-motion library with applications in light-harvesting, quantum control and single-molecule electronics *Phys. Rev. Res.* **5** 013181
[104] Johansson J, Nation P and Nori F 2012 QuTiP: an open-source Python framework for the dynamics of open quantum systems *Comput. Phys. Commun.* **183** 1760
[105] Johansson J, Nation P and Nori F 2013 QuTiP 2: a Python framework for the dynamics of open quantum systems *Comput. Phys. Commun.* **184** 1234
[106] Haegeman J, Lubich C, Oseledets I, Vandereycken B and Verstraete F 2016 Unifying time evolution and optimization with matrix product states *Phys. Rev. B* **94** 165116
[107] Chanda T, Sierant P and Zakrzewski J 2020 Time dynamics with matrix product states: many-body localization transition of large systems revisited *Phys. Rev. B* **101** 035148
[108] Ng N, Park G, Millis A J, Chan G K-L and Reichman D R 2023 Real-time evolution of Anderson impurity models via tensor network influence functionals *Phys. Rev. B* **107** 125103
[109] Thoenniss J, Sonner M, Lerose A and Abanin D A 2023 Efficient method for quantum impurity problems out of equilibrium *Phys. Rev. B* **107** L201115
[110] Pollock F A, Rodríguez-Rosario C, Frauenheim T, Paternostro M and Modi K 2018 Non-Markovian quantum processes: complete framework and efficient characterization *Phys. Rev. A* **97** 012127
[111] Milz S and Modi K 2021 Quantum stochastic processes and quantum non-Markovian phenomena *PRX Quantum* **2** 030201
[112] Woods M P, Cramer M and Plenio M B 2015 Simulating bosonic baths with error bars *Phys. Rev. Lett.* **115** 130401
[113] Woods M P and Plenio M B 2016 Dynamical error bounds for continuum discretisation via Gauss quadrature rules–a Lieb-Robinson bound approach *J. Math. Phys.* **57** 022105
[114] Lerose A, Sonner M and Abanin D A 2023 Overcoming the entanglement barrier in quantum many-body dynamics via space-time duality *Phys. Rev. B* **107** L060305
[115] Rams M M and Zwolak M 2020 Breaking the entanglement barrier: tensor network simulation of quantum transport *Phys. Rev. Lett.* **124** 137701
[116] Foligno A, Zhou T and Bertini B 2023 Temporal entanglement in chaotic quantum circuits *Phys. Rev. X* **13** 041008
[117] Garcia-Gaitan F and Nikolić B K 2024 Fate of entanglement in magnetism under Lindbladian or non-Markovian dynamics and conditions for their transition to Landau-Lifshitz-Gilbert classical dynamics *Phys. Rev. B* **109** L180408
[118] Trivedi R and Cirac J I 2022 Transitions in computational complexity of continuous-time local open quantum dynamics *Phys. Rev. Lett.* **129** 260405
[119] Nüeler A, Tamascelli D, Smirne A, Lim J, Huelga S F and Plenio M B 2022 Fingerprint and universal Markovian closure of structured bosonic environments *Phys. Rev. Lett.* **129** 140604
[120] Dunnett A J and Chin A W 2021 Efficient bond-adaptive approach for finite-temperature open quantum dynamics using the one-site time-dependent variational principle for matrix product states *Phys. Rev. B* **104** 214302
[121] Nuomin H, Beratan D N and Zhang P 2022 Improving the efficiency of open-quantum-system simulations using matrix product states in the interaction picture *Phys. Rev. A* **105** 032406
[122] Vidal G 2003 Efficient classical simulation of slightly entangled quantum computations *Phys. Rev. Lett.* **91** 147902
[123] Takahashi Y and Umezawa H 1996 Thermo field dynamics *Int. J. Mod. Phys. B* **10** 1755
[124] Gautschi W 2005 Orthogonal polynomials in Matlab *J. Comput. Appl. Math.* **178** 215
[125] Haegeman J, Cirac J I, Osborne T J, Pižorn I, Verschelde H and Verstraete F 2011 Time-dependent variational principle for quantum lattices *Phys. Rev. Lett.* **107** 070601
[126] Lubich C, Oseledets I V and Vandereycken B 2015 Time integration of tensor trains *SIAM J. Numer. Anal.* **53** 917
[127] Paeckel S, Köhler T, Swoboda A, Manmana S R, Schollwöck U and Hubig C 2019 Time-evolution methods for matrix-product states *Ann. Phys.* **411** 167998
[128] Bajpai U, Suresh A and Nikolić B K 2021 Quantum many-body states and Greenś functions of nonequilibrium electron-magnon systems: Localized spin operators versus their mapping to Holstein-Primakoff bosons *Phys. Rev. B* **104** 184425
[129] Auerbach A 1994 *Interacting Electrons and Quantum Magnetism* (Springer)

[130] Auerbach A and Arovas D P 2008 Schwinger bosons approaches to quantum antiferromagnetism (arXiv:0809.4836)
[131] Zhang S-S, Ghioldi E A, Manuel L O, Trumper A E and Batista C D 2022 Schwinger boson theory of ordered magnets *Phys. Rev. B* **105** 224404
[132] Gohlke M, Corticelli A, Moessner R, McClarty P A and Mook A 2023 Spurious symmetry enhancement in linear spin wave theory and interaction-induced topology in magnons *Phys. Rev. Lett.* **131** 186702
[133] Li Q-S, Liu H-Y, Wang Q, Wu Y-C and Guo G-P 2022 A unified framework of transformations based on the Jordan-Wigner transformation *J. Chem. Phys.* **157** 134104
[134] Aarts G and Berges J 2002 Classical aspects of quantum fields far from equilibrium *Phys. Rev. Lett.* **88** 041603
[135] Stefanucci G and van Leeuwen R 2025 *Nonequilibrium Many-Body Theory of Quantum Systems: A Modern Introduction* (Cambridge University Press)
[136] Schlünzen N, Hermanns S, Scharnke M and Bonitz M 2019 Ultrafast dynamics of strongly correlated fermions—nonequilibrium Green functions and selfenergy approximations *J. Phys.: Condens. Matter* **32** 103001
[137] Schlünzen N, Joost J-P, Heidrich-Meisner F and Bonitz M 2017 Nonequilibrium dynamics in the one-dimensional Fermi-Hubbard model: comparison of the nonequilibrium Green-functions approach and the density matrix renormalization group method *Phys. Rev. B* **95** 165139
[138] Hyrkäs M J, Karlsson D and van Leeuwen R 2019 Contour calculus for many-particle functions *J. Phys. A: Math. Theor.* **52** 215303
[139] Altland A and Simons B 2023 *Condensed Matter Field Theory* (Cambridge University Press)
[140] Takei S 2019 Spin transport in an electrically driven magnon gas near Bose-Einstein condensation: Hartree-Fock-Keldysh theory *Phys. Rev. B* **100** 134440
[141] Mahfouzi F and Nikolić B K 2014 Signatures of electron-magnon interaction in charge and spin currents through magnetic tunnel junctions: a nonequilibrium many-body perturbation theory approach *Phys. Rev. B* **90** 045115
[142] Berges J 2002 Controlled nonperturbative dynamics of quantum fields out of equilibrium *Nucl. Phys. A* **699** 847
[143] Burchards A G, Feldmeier J, Schuckert A and Knap M 2022 Coupled hydrodynamics in dipole-conserving quantum systems *Phys. Rev. B* **105** 205127
[144] Kronenwett M and Gasenzer T 2011 Far-from-equilibrium dynamics of an ultracold Fermi gas *Appl. Phys. B* **102** 469
[145] Savary L and Balents L 2016 Quantum spin liquids: a review *Rep. Prog. Phys.* **80** 016502
[146] Meirinhos F, Kajan M, Kroha J and Bode T 2022 Adaptive numerical solution of Kadanoff-Baym equations *SciPost Phys. Core* **5** 030
[147] Blommel T, Gardner D J, Woodward C S and Gull E 2024 Adaptive time stepping for the two-time integro-differential Kadanoff-Baym equations *Phys. Rev. B* **110** 205134
[148] Inayoshi K, Środa M, Kauch A, Werner P, Shinaoka H 2025 A causality-based divide-and-conquer algorithm for nonequilibrium Green's function calculations with quantics tensor trains (arXiv:2509.15028)
[149] Fernández Y N *et al* 2025 Learning tensor networks with tensor cross interpolation: new algorithms and libraries *SciPost Phys.* **18** 104
[150] Garny M and Müller M M 2009 Kadanoff-Baym equations with non-Gaussian initial conditions: the equilibrium limit *Phys. Rev. D* **80** 085011
[151] van Leeuwen R and Stefanucci G 2013 Equilibrium and nonequilibrium many-body perturbation theory: a unified framework based on the Martin-Schwinger hierarchy *J. Phys.: Conf. Ser.* **427** 012001
[152] Carrington M E, Meggison B A and Pickering D 2016 2PI effective action at four loop order in φ^4 theory *Phys. Rev. D* **94** 025018
[153] Chakraborty A, Gorantla P and Sensarma R 2019 Nonequilibrium field theory for dynamics starting from arbitrary athermal initial conditions *Phys. Rev. B* **99** 054306
[154] Käding C and Pitschmann M 2023 New method for directly computing reduced density matrices *Phys. Rev. D* **107** 016005
[155] Reyes-Osorio F and Nikolić B K 2024 Gilbert damping in metallic ferromagnets from Schwinger-Keldysh field theory: intrinsically nonlocal, nonuniform and made anisotropic by spin-orbit coupling *Phys. Rev. B* **109** 024413
[156] Verstraten R C, Ludwig T, Duine R A and Morais Smith C 2023 Fractional Landau-Lifshitz-Gilbert equation *Phys. Rev. Res.* **5** 033128
[157] Anders J, Sait C R J and Horsley S A R 2022 Quantum Brownian motion for magnets *New J. Phys.* **24** 033020
[158] Landau L D and Lifshitz E M 1935 On the theory of the dispersion of magnetic permeability in ferromagnetic bodies *Phys. Z. Sowjetunion* **8** 153
[159] Bajpai U and Nikolić B 2019 Time-retarded damping and magnetic inertia in the Landau-Lifshitz-Gilbert equation self-consistently coupled to electronic time-dependent nonequilibrium Green functions *Phys. Rev. B* **99** 134409
[160] Reyes-Osorio F and Nikolic B K 2025 Bringing light into the Landau-Lifshitz-Gilbert equation: consequences of its fractal non-Markovian memory kernel for optically induced magnetic inertia and magnons (arXiv:2504.17769)
[161] Bhattacharjee S, Nordström L and Fransson J 2012 Atomistic spin dynamic method with both damping and moment of inertia effects included from first principles *Phys. Rev. Lett.* **108** 057204
[162] Fauth G, Berges J and Di Piazza A 2021 Collisional strong-field QED kinetic equations from first principles *Phys. Rev. D* **104** 036007
[163] Chakraborty A and Sensarma R 2018 Power-law tails and non-Markovian dynamics in open quantum systems: an exact solution from Keldysh field theory *Phys. Rev. B* **97** 104306
[164] Saslow W M 2009 Landau-Lifshitz or Gilbert damping? that is the question *J. Appl. Phys.* **105** 07D315
[165] Hur K L 2008 Entanglement entropy, decoherence and quantum phase transitions of a dissipative two-level system *Ann. Phys.* **323** 2208–40
[166] De Filippis G, de Candia A, Cangemi L M, Sassetti M, Fazio R and Cataudella V 2020 Quantum phase transitions in the spin-boson model: Monte Carlo method versus variational approach à la Feynman *Phys. Rev. B* **101** 180408
[167] Sachdev S 2011 *Quantum Phase Transitions* (Cambridge University Press)
[168] Landi G T, Poletti D and Schaller G 2022 Nonequilibrium boundary-driven quantum systems: models, methods and properties *Rev. Mod. Phys.* **94** 045006
[169] Göhmann F, Kozlowski K K, Sirker J and Suzuki J 2022 Spin conductivity of the XXZ chain in the antiferromagnetic massive regime *SciPost Phys.* **12** 158
[170] Mendoza-Arenas J J, Al-Assam S, Clark S R and Jaksch D 2013 Heat transport in the XXZ spin chain: from ballistic to diffusive regimes and dephasing enhancement *J. Stat. Mech.* 07007

[171] Puig von Friesen M, Verdozzi C and Almbladh C-O 2010 Kadanoff-Baym dynamics of Hubbard clusters: performance of many-body schemes, correlation-induced damping and multiple steady and quasi-steady states *Phys. Rev. B* **82** 155108
[172] Koksma J F, Prokopec T and Schmidt M G 2011 Decoherence in an interacting quantum field theory: thermal case *Phys. Rev. D* **83** 085011
[173] Park T J and Light J C 1986 Unitary quantum time evolution by iterative Lanczos reduction *J. Chem. Phys.* **85** 5870
[174] Stoudenmire E and White S R 2012 Studying two-dimensional systems with the density matrix renormalization group *Annu. Rev. Condens. Matter Phys.* **3** 111
[175] Cirac J I, Pérez-García D, Schuch N and Verstraete F 2021 Matrix product states and projected entangled pair states: concepts, symmetries, theorems *Rev. Mod. Phys.* **93** 045003
[176] Del Re L, Rost B, Kemper A F and Freericks J K 2020 Driven-dissipative quantum mechanics on a lattice: Simulating a fermionic reservoir on a quantum computer *Phys. Rev. B* **102** 125112
[177] Nikolaeva A S, Kiktenko E O and Fedorov A K 2024 Efficient realization of quantum algorithms with qudits *EPJ Quantum Technol.* **11** 43
[178] Kasahara Y *et al* 2018 Majorana quantization and half-integer thermal quantum Hall effect in a Kitaev spin liquid *Nature* **559** 227
[179] Kaye J and Golež D 2021 Low rank compression in the numerical solution of the nonequilibrium Dyson equation *SciPost Phys.* **10** 091
[180] Zhu Y, Yin J, Reeves C, Yang C and Vlcek V 2025 Predicting nonequilibrium Green's function dynamics and photoemission spectra via nonlinear integral operator learning *Mach. Learn.: Sci. Technol.* **6** 015027